Physics of Fluids

Locomotion of a rotating cylinder pair with periodic gaits at low Reynolds numbers

Lingbo Ji (冀凌波)[1] and Wim M. van Rees[1, a)]
Department of Mechanical Engineering
Massachusetts Institute of Technology
Cambridge, MA 02139, USA

(Dated: 10 September 2020)

We consider the periodic gaits of a microswimmer formed by two rotating cylinders, placed apart at a fixed width. Through a combination of theoretical arguments and numerical simulations, we derive semi-analytic expressions for system's instantaneous translational and rotational velocities, as a function of the rotational speeds of each cylinder. We can then integrate these relations in time to find the speed and efficiency of the swimmer for any imposed gait. Here we focus particularly on identifying the periodic gaits that lead to the highest efficiency. To do so, we consider three stroke parametrizations in detail: alternating strokes, where only one cylinder rotates at a time; titled rectangle strokes, that combine co- and counter-rotation phases; and smooth strokes represented through a set of Fourier series coefficients. For each parametrization we compute maximum efficiency solutions using a numerical optimization approach. We find that the parameters of the global optimum, and the associated efficiency value, depend on the average mechanical input power. The efficiency asymptotes towards that of a steadily counter-rotating cylinder pair as the input power increases. Finally, we address a possible three-dimensional extension of this system by evaluating the efficiency of a counter-rotating three-dimensional (3D) cylinder pair with spherical end caps. We conclude that the counter-rotating cylinder pair combines competitive efficiency values and offer high versatility with simplicity of geometry and actuation, and thus could be a possible basis for engineered microswimmers.

I. INTRODUCTION

Locomotion at low Reynolds numbers has relevance in nature and engineering. In nature, the swimming of micro-scale organisms such as bacteria, algae, and protozoa is of interest to understand their proliferation and interactions[1]. In bio-engineering and healthcare, the viability of micro-robots is of interest for delivering drugs through the bloodstream, or as a way to sense or diagnose a patient's condition[2,3].

At these Reynolds numbers, viscous effects dominate over inertial ones, so that the motion of such swimmers is governed by the linear time-invariant Stokes equations. Starting from the seminal work of Purcell [4], a large collection of theoretical, archetypal swimming models have been proposed that rely on some combination of shape transformations. The conceptually simplest models are based on linked rigid bodies with a small number of discrete degrees-of-freedom, such as Purcell's three-link swimmer[4] and the three-sphere swimmer[5], which also have been experimentally realized[6,7]. More complex models involve continuous surface deformations such as undulations[8,9] or tank-threading approaches[10,11].

In two dimensions, a geometrically simple model involves two disks whose centers are fixed at a set distance, each of which rotates about its own axis. This swimmer can be interpreted as a two-dimensional (2D) cross-section of Purcell's tank-threading torus[4], or alternatively as a cross-section of a pair of infinitely long three-dimensional cylinders. For the latter interpretation, the swimming gait is fully captured with rigid body rotations of each cylinder, which could provide an attractively simple conceptual basis for robotic microswimmers.

a)Electronic mail: wvanrees@mit.edu

Compared to other model swimmers the cylinder pair is unique in that, by steadily counter-rotating the cylinders, it can achieve a steady rectilinear locomotion. This case has been analysed by Leshansky and Kenneth [11], who have further provided analytic solutions for the counter-rotating cylinder pair's behavior. They showed that the cylinder pair will undergo a linear translation with speed $a^2\Omega/W$, with a the cylinder radius, W the center-to-center width, and Ω the angular rotation speed of each cylinder. By changing the reference frame, this result can also be found in the century-old work by Jeffery [12]. The behavior of the counter-rotating cylinder pair in Reynolds numbers of $\mathcal{O}(10)$–$\mathcal{O}(100)$ was undertaken in van Rees, Novati, and Koumoutsakos [13] by numerically solving the Navier-Stokes equations.

Our work here remains in the Stokes regime, and is focused on broadening the space of actuation patterns to include unsteady periodic gaits, and investigate the resulting motion patterns. We expect our results to explore the versatility of the system and learn about a new set of gaits that can result in rectilinear locomotion. Though the efficiency of unsteady periodic gaits will always be bounded by that of the steady counter-rotating solution, our analysis can aid comparisons with other model systems, as well as inform potential experimental applications that require maneuverability or periodic actuation patterns.

To achieve this goal, in Section II we first present a combined theoretical/numerical approach where we use the method of regularized Stokeslets[14] to extract geometry-dependent coefficients, and then use a semi-analytical approach to efficiently compute the performance for individual gaits. This enables us to perform numerical optimizations of the cylinder pair gaits, similar to the approach of Tam and Hosoi [15], with low computational cost. In Section III we discuss the three types of gaits that we consider here, correspond-

ing to squares, tilted-rectangles and smooth closed curves in the rotation-angle phase space, respectively. The results for the physical trajectories and efficiencies for these gaits are analyzed in Section IV. In Section V we discuss the extension of the 2D cylinder pair system to a 3D counter-rotating cylinder pair, and explore for the first time the efficiency of this simple system to three dimensions.

II. PROBLEM SETUP

A. Geometry and kinematics

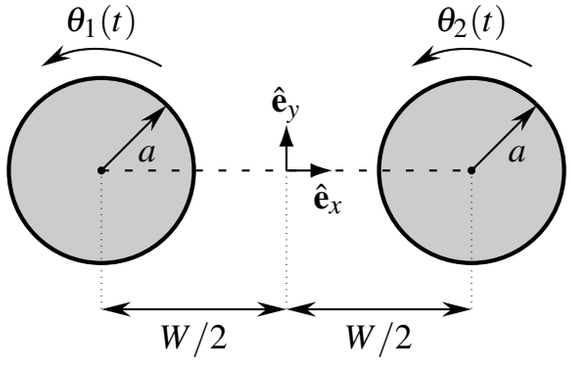

FIG. 1. Sketch of the problem setup

Our geometry consists of two identical cylinders with radius a, positioned side by side at a fixed distance W, as sketched in Fig. 1. The two cylinders are rotated about their own centers by angles $\theta_1(t)$ and $\theta_2(t)$ respectively, with corresponding angular velocities $\dot{\theta}_1(t)$ and $\dot{\theta}_2(t)$. To ensure periodic gaits, we impose the constraint that the net angle rotated by each cylinder is zero after the gait period T, that is

$$\int_0^T \dot{\theta}_1(t)\,\mathrm{d}t = \int_0^T \dot{\theta}_2(t)\,\mathrm{d}t = 0. \tag{1}$$

For convenience, we will set $T = 1$ throughout the rest of this work, and focus on a single geometry characterized by $W/a = 4$.

B. Method of regularized Stokeslets

For the very low Reynolds numbers considered here the fluid flow is governed by the Stokes equations:

$$\mu\nabla^2\mathbf{u} = \nabla p - \mathbf{f} \tag{2}$$

$$\nabla\cdot\mathbf{u} = 0 \tag{3}$$

where $\mathbf{u}$ denotes the velocity, p denotes the pressure and $\mathbf{f}$ is the external forcing, which in our case is responsible for enforcing the no-slip boundary conditions on the flow at the surface of the cylinders.

To solve the Stokes flow around the cylinder pair, we use the method of regularized-Stokeslets in two-dimensions[14]. In this method, the boundary element problem is discretized using a set of singular forces distributed along the surface of the object. Using a regularization of the forces with characteristic length scale ε, a force field composed of N discrete forces can be expressed as $\mathbf{f}(\mathbf{x}) = \sum_{k=1}^{N}\mathbf{f}_k\phi_\varepsilon(\mathbf{x}-\mathbf{y}_k)$, where the index k corresponds to the point at location $\mathbf{y}_k$ on the boundary of the object, with associated force vector $\mathbf{f}_k$. Following Cortez[14], we choose the cutoff function to be

$$\phi_\varepsilon(\mathbf{x}-\mathbf{y}) = \frac{3\varepsilon^3}{2\pi(|\mathbf{x}-\mathbf{y}|^2+\varepsilon^2)^{5/2}} \tag{4}$$

with the regularization parameter ε. Using this approximation, the velocity field at any location $\mathbf{x}$ in the domain or on the boundary, can be written as a discrete convolution[14]

$$\begin{aligned}\mathbf{u}(\mathbf{x}) = \sum_{k=1}^{N}\Bigg\{&\frac{-\mathbf{f}_k}{4\pi\mu}\left[\ln\left(r_{k,\varepsilon}+\varepsilon\right) - \frac{\varepsilon\left(r_{k,\varepsilon}+2\varepsilon\right)}{\left(r_{k,\varepsilon}+\varepsilon\right)r_{k,\varepsilon}}\right]\\ &+\frac{1}{4\pi\mu}\left(\mathbf{f}_k\cdot\boldsymbol{r}_k\right)\boldsymbol{r}_k\left[\frac{r_{k,\varepsilon}+2\varepsilon}{\left(r_{k,\varepsilon}+\varepsilon\right)^2 r_{k,\varepsilon}}\right]\Bigg\}\end{aligned} \tag{5}$$

where $\boldsymbol{r}_k = \mathbf{x}-\mathbf{y}_k$, $r_k = |\boldsymbol{r}_k|$, and its regularization $r_{k,\varepsilon} = \sqrt{r_k^2+\varepsilon^2}$.

If the velocity on the boundary of the object is known, the expression above leads to a $2N\times 2N$ algebraic system of equations that can be inverted for $\mathbf{f}_k$. Using $\mathbf{f}_k$, the velocity field at any point in the domain can then be evaluated if desired.

In our case, we consider a self-propelled body with imposed wall rotational velocity. In the body-fixed coordinate, the rigid-body motion is described by $\mathbf{u}_{\mathrm{com}} = (u_{\mathrm{com}}, v_{\mathrm{com}})$ and $\dot{\boldsymbol{\theta}}_{\mathrm{com}} = \dot{\theta}_{\mathrm{com}}\hat{\mathbf{e}}_z$, which denote the linear and angular velocities of the cylinder pair's center of mass respectively. For our geometry, we can directly write the velocity on cylinder i at angle θ_i as

$$\begin{aligned}\mathbf{u}_i = \mathbf{u}_{\mathrm{com}} &+ s_i\frac{W}{2}\dot{\theta}_{\mathrm{com}}\begin{pmatrix}-\sin(\theta_{\mathrm{com}})\\ \cos(\theta_{\mathrm{com}})\end{pmatrix}\\ &+ a(\dot{\theta}_{\mathrm{com}}+\dot{\theta}_i)\begin{pmatrix}-\sin(\theta_{\mathrm{com}}+\theta_i)\\ \cos(\theta_{\mathrm{com}}+\theta_i)\end{pmatrix},\end{aligned} \tag{6}$$

where $i = 1,2$, $s_1 = -1$, and $s_2 = +1$.

Furthermore, since the cylinder pair is self-propelled in a Stokes flow, the net force and torque on the system are zero:

$$\int_\Gamma \mathbf{f}\,\mathrm{d}s = 0, \tag{7}$$

$$\int_\Gamma \mathbf{x}\times\mathbf{f}\,\mathrm{d}s = 0. \tag{8}$$

Equations (7) and (8) represent 3 scalar constraint equations on the forces that supplement Eq. (6). This then results in a closed linear system of size $(2N+3)\times(2N+3)$ for the unknowns $\mathbf{f}_k$ as well as the center of mass translational and angular velocities. Given instantaneous angular velocities $\dot{\theta}_1(t)$

and $\dot{\theta}_2(t)$, the system is closed and we can solve for the cylinder pair's translational and angular velocities. Given those, a numerical integration in time provides the next center of mass location and orientation. By iterating these steps we can find the trajectory of the cylinder pair for an entire swimming cycle, given the time evolution of $\dot{\theta}_1(t)$ and $\dot{\theta}_2(t)$.

C. Efficiency definition

In this work we wish to investigate the hydrodynamic swimming efficiency of the cylinder pair with periodic gaits. Typically the swimming efficiency is defined as the average rate of useful work to the average mechanical power required during a swimming cycle:

$$\eta' = \frac{\Phi_{\text{useful}}}{\bar{\Phi}}, \tag{9}$$

where Φ_{useful} is the power required to drag the swimmer in a fixed configuration at the average velocity that would have been achieved in a free-swimming cycle, and $\bar{\Phi}$ is the average mechanical power expended in a swimming period.

In two-dimensional Stokes flow, though the self-propulsion (swimming) problem is well-posed, the dragging problem is not[1]. This makes the above definition of Φ_{useful} inappropriate for our two-dimensional configuration. Instead, we follow Avron, Gat, and Kenneth [16] to provide the following alternative measure of efficiency for a 2D swimmer in Stokes flow:

$$\eta = \frac{4\pi\mu\bar{\mathbf{u}}^2}{\bar{\Phi}}, \tag{10}$$

where $\bar{\mathbf{u}}$ is the average velocity of the swimmer in one period and $\bar{\Phi}$ still the average mechanical power expended in one period. Maximizing this efficiency can be interpreted as minimizing the energy dissipated per unit swimming distance at fixed average speed, or conversely as maximizing the distance traveled for a given average power expense.

For the specific geometry considered here ($W = 4a$), an analytic result of the steady-state efficiency for a counter-rotating cylinder pair was found in Leshansky and Kenneth [11] to be $\eta = \frac{1}{2}\left(\frac{a}{W}\right)^2$, which for our choice of geometry ($W/a = 4$) gives $1/32 = 0.03125$.

D. Symmetries

Since the Stokes equations are linear and time-independent, for a fixed geometric configuration the center of mass velocity and rotation will vary linearly with the deformation velocities[1,17]. In particular, for our system, we can decompose, at any time, the stroke velocities $\dot{\theta}_1(t)$ and $\dot{\theta}_2(t)$ into a symmetric and an anti-symmetric component:

$$\dot{\theta}_\times = \frac{1}{2}\left(\dot{\theta}_1 - \dot{\theta}_2\right) \tag{11}$$

$$\dot{\theta}_\parallel = \frac{1}{2}\left(\dot{\theta}_1 + \dot{\theta}_2\right), \tag{12}$$

where $\dot{\theta}_\times$ and $\dot{\theta}_\parallel$ correspond to counter-rotation (symmetric with respect to the line separating the cylinders) and co-rotation (anti-symmetric) of the cylinders, respectively. Based on the symmetries of the problem, for a cylinder pair as oriented in Fig. 1, we pose that the center-of-mass velocity corresponding to counter-rotation can only have a component along the local $\hat{\mathbf{e}}_y$ direction, so that the local component $u_{\text{com}} = 0$ for any gait. Furthermore, because of the linearity of the problem, we have

$$v_{\text{com}} = A_1(\dot{\theta}_1 - \dot{\theta}_2), \tag{13}$$

where A_1 is a geometry-dependent proportionality constant. As mentioned before, it has been found that for the counter-rotating case $v_{\text{com}} = a^2\Omega/W$[11,12], where Ω is the angular speed of each cylinder, so that we can directly evaluate $A_1 = a^2/2W$.

Similarly, the center-of-mass velocity corresponding to co-rotation can only have a rotational component, so that

$$\dot{\theta}_{\text{com}} = A_2(\dot{\theta}_1 + \dot{\theta}_2) \tag{14}$$

with A_2 the proportionality factor. Further, the instantaneous mechanical power is a quadratic function of $\dot{\theta}_1(t)$, $\dot{\theta}_2(t)$, which, taking into account the symmetries of the problem, reduces to

$$\Phi_{\text{mech}} = B_1(\dot{\theta}_1^2 + \dot{\theta}_2^2) + B_2\dot{\theta}_1\dot{\theta}_2, \tag{15}$$

where B_1 and B_2 are geometry-dependent constants.

We can use the method of regularized Stokeslets to perform a series of simulations of different combinations of $\dot{\theta}_1$ and $\dot{\theta}_2$, and determine the constants A_1, A_2, B_1, and B_2 through a data-fit of the results. The computation of the numerical values of A_1, A_2, B_1, B_2 as a function of the separation length W is discussed in Appendix A.

With the numerical values of these constants known, we can find the velocity of the center of mass for any combination of $\dot{\theta}_1$ and $\dot{\theta}_2$ simply by using relationships in Eq. (13) and (14). This approach greatly reduces the numerical costs of computing the cylinder pair's trajectory for a given gait, since it avoids the necessity to solve the Stokes flow at each time step.

III. PARAMETRIZATION OF THE PERIODIC GAITS

In this section we explain the parametrization of the three gaits considered here, corresponding to squares, tilted rectangles, and titled smooth parametric curves in the phase-space (Fig. 2, multimedia view). For the first two, we demonstrate that we can provide closed-form expressions of the efficiency in terms of the gait parameters and average mechanical work $\bar{\Phi}$. For the smooth parametric curve, we explain the parametrization and optimization approach.

A. Alternating strokes

Purcell's three-link swimmer is characterized by a stroke where only one of the left and right arm of the swimmer moves

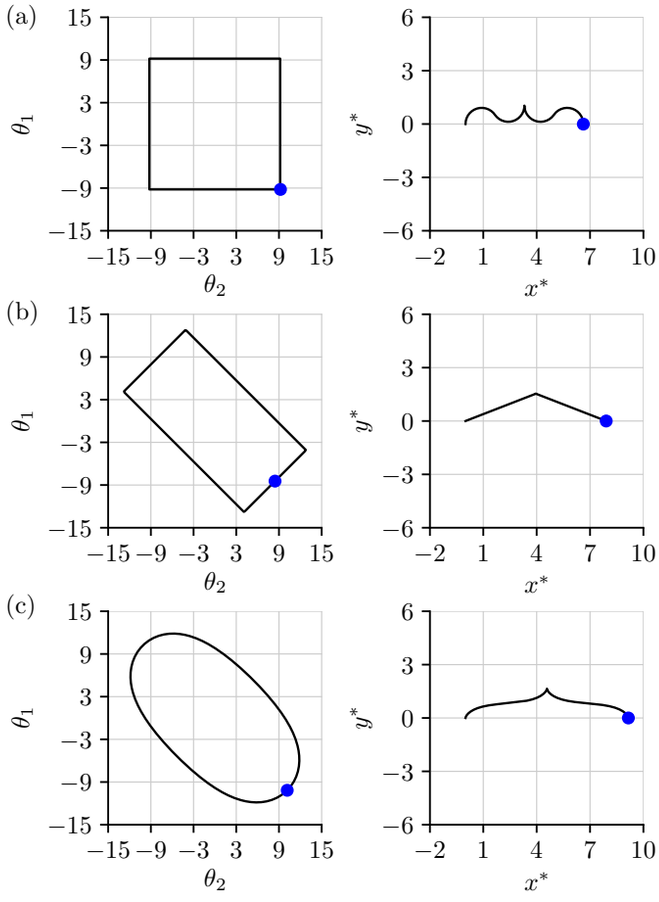

FIG. 2. Phase space diagrams and physical trajectories for the three types of gaits considered here, plotted for the same nondimensional average mechanical power $\bar{\Phi}^* = \bar{\Phi}/\left(\mu a^2/T^2\right) = 10^4$. The efficiencies for the (a) alternating stroke, (b) tilted-rectangle stroke, and (c) smooth parametric optimization are 0.0088, 0.0125, 0.0167, respectively. The blue dots in the phase space (left column) denote the start and end points of the phase diagrams; the blue dots in the physical space (right column) denote the end points of the physical trajectories. All lengths are scaled with cylinder radius a. (Multimedia view).

at a time, resulting in square shapes in the phase space[4]. For our case of a cylinder pair, we define corresponding alternating strokes for which the two cylinders alternatively rotate by an angular amplitude γ, with constant angular speed. This leads to squares with side length 2γ in the phase space. To achieve such alternating strokes, we parameterize the angular velocities as

$$\left(\dot{\theta}_1(t), \dot{\theta}_2(t)\right) = \begin{cases} \left(\dot{\theta}_{\text{alt}}, 0\right), & 0 < t \le 1/4 \\ \left(0, -\dot{\theta}_{\text{alt}}\right), & 1/4 < t \le 1/2 \\ \left(-\dot{\theta}_{\text{alt}}, 0\right), & 1/2 < t \le 3/4 \\ \left(0, \dot{\theta}_{\text{alt}}\right), & 3/4 < t \le 1 \end{cases} \tag{16}$$

where $\dot{\theta}_{\text{alt}} = 8\gamma$. From Eq. (15), the instantaneous mechanical power $\Phi = B_1 \dot{\theta}_{\text{alt}}^2$ is constant throughout the cycle and depends only on the rotation speed $\dot{\theta}_{\text{alt}}$. We can use this to express the efficiency directly in terms of the average mechanical power $\bar{\Phi}$ (see Appendix B), which gives the analytic expression for the efficiency of this stroke as

$$\eta_{\text{alt}}(\bar{\Phi}) = \frac{64\pi\mu}{\bar{\Phi}} \left(\frac{A_1}{A_2}\right)^2 \left[1 - \cos\left(\frac{A_2}{4}\sqrt{\frac{\bar{\Phi}}{B_1}}\right)\right]^2. \tag{17}$$

B. Tilted-Rectangle strokes

With the aim of constructing a simple periodic gait with high efficiency, we propose combining the two most basic rotation patterns of the cylinder pair: counter-rotation and co-rotation. Alternating these patterns results in rectangles tilted at 45° in the phase space, and so we refer to these strokes as tilted-rectangle (TR) strokes. We denote the constant angular speed of the cylinders during the counter-rotation and co-rotation phases as $\dot{\theta}_\times$ and $\dot{\theta}_\parallel$, respectively. The time fraction spent in the counter-rotating part of the gait is $t_\times$. The angular velocities can thus be written as

$$\left(\dot{\theta}_1(t), \dot{\theta}_2(t)\right) = \begin{cases} \left(\dot{\theta}_\parallel, \dot{\theta}_\parallel\right), & 0 < t \le (1-t_\times)/4 \\ \left(\dot{\theta}_\times, -\dot{\theta}_\times\right), & (1-t_\times)/4 < t \le (1+t_\times)/4 \\ \left(-\dot{\theta}_\parallel, -\dot{\theta}_\parallel\right), & (1+t_\times)/4 < t \le (3-t_\times)/4 \\ \left(-\dot{\theta}_\times, \dot{\theta}_\times\right), & (3-t_\times)/4 < t \le (3+t_\times)/4 \\ \left(\dot{\theta}_\parallel, \dot{\theta}_\parallel\right), & (3+t_\times)/4 < t \le 1 \end{cases} \tag{18}$$

The gait is completely described by the choice of $\dot{\theta}_\parallel$, $\dot{\theta}_\times$ and the time fraction spent in the counter-rotation phases $t_\times$. Using equation Eq. (15), we have for this case $\bar{\Phi} = (2B_1 + B_2)\dot{\theta}_\parallel^2(1-t_\times) + (2B_1 - B_2)\dot{\theta}_\times^2 t_\times$, and so we can alternatively replace $t_\times$ with $\bar{\Phi}$ as the third free parameter.

The physical trajectories for the TR strokes simply consist of two straight line segments of length L corresponding to the counter-rotation phases (Fig. 2, middle (Multimedia view)). The angle α between the length segments is determined by the rate and duration of the co-rotation phase. We can directly write down the definitions of L and α in terms of the control parameters, leading to

$$L = A_1 |\dot{\theta}_\times| t_\times, \tag{19}$$

$$\alpha = A_2 |\dot{\theta}_\parallel| (1 - t_\times) \tag{20}$$

where

$$t_\times = \frac{\bar{\Phi} - (2B_1 + B_2)\dot{\theta}_\parallel^2}{(2B_1 - B_2)\dot{\theta}_\times^2 - (2B_1 + B_2)\dot{\theta}_\parallel^2}. \tag{21}$$

The efficiency of the stroke is then

$$\eta_{\text{TR}} = \frac{4\pi\mu(2L\sin(\alpha/2))^2}{\bar{\Phi}}, \tag{22}$$

with L and α defined above.

A special case that is worth considering occurs when the center of mass rotation equals $\alpha = \pi$, so that the trajectory is a straight line. We can directly apply this constraint to the efficiency definition to eliminate $\dot{\theta}_{\|}$ to get

$$\eta_{\mathrm{TR}} = \frac{16\pi\mu(A_1|\dot{\theta}_\times|t_\times)^2}{\bar{\Phi}}. \tag{23}$$

C. Smooth parametric strokes

Under the linear and time-independent Stokes equations, our system has two mirror symmetries that correspond to reflection and rotation of the gait. In phase-space, these symmetries are given by the straight lines described by $\theta_1 = \theta_2$ and $\theta_1 = -\theta_2$. We expect optimal strokes to satisfy these symmetries and, following Tam and Hosoi [15], we therefore parametrize the rotation rates using Fourier cosine and sine series in a frame $(\hat{\theta}_1,\ \hat{\theta}_2)$ that is rotated clockwise by $\pi/4$:

$$\hat{\theta}_1 = \sum_{p=1,\mathrm{odd}}^{M} a_p \sin(2\pi pt) \tag{24}$$

$$\hat{\theta}_2 = \sum_{p=1,\mathrm{odd}}^{M} b_p \cos(2\pi pt). \tag{25}$$

To evaluate the values of (θ_1, θ_2), we transform the expressions back to the original frame $(\theta_1,\ \theta_2)$ to obtain

$$\theta_1(t) = \frac{1}{\sqrt{2}} \sum_{p=1,\ \mathrm{odd}}^{M} a_p \sin(2\pi pt) - b_p \cos(2\pi pt) \tag{26}$$

$$\theta_2(t) = \frac{1}{\sqrt{2}} \sum_{p=1,\ \mathrm{odd}}^{M} a_p \sin(2\pi pt) + b_p \cos(2\pi pt). \tag{27}$$

We again rely on the expressions (13), (14), and (15) to efficiently compute the center-of-mass velocities and power during the stroke for any set of coefficients $\{a_p, b_p\}$, and integrate these to find the efficiency. Since we have no closed-form solution, we use numerical optimization to find the values of the Fourier coefficients which give the maximum swimming efficiency, for a range of values of nondimensional average mechanical power $\bar{\Phi}^* = \bar{\Phi}/(\mu a^2/T^2)$. The optimization is performed using the MATLAB built-in function fminunc, which finds a minimum of a unconstrained multivariable function using the BFGS Quasi-Newton method with a cubic line search procedure. To fix the value of $\bar{\Phi}^*$ in each optimization, the trial input $\{a_p, b_p\}$ is first scaled to get the desired value of $\bar{\Phi}^*$. For example, if the input $\{a_p, b_p\}$ leads to an average mechanical power $\bar{\Phi}^*$ and the desired value is $\bar{\Phi}^*_0$, then according to Eq. 15 we can rescale the coefficients to $\{Ca_p, Cb_P\}$, with the scale factor $C = \sqrt{\bar{\Phi}^*_0/\bar{\Phi}^*}$. Finally, we increase the number of coefficients M until the optimal stroke has converged, which is further detailed in Appendix D.

IV. OPTIMAL GAITS

The efficiencies η versus the nondimensional average mechanical power $\bar{\Phi}^*$ for the three different types of strokes are plotted in Fig. 3. We also plot the analytic result for the efficiency of the steady-state counter-rotating cylinder pair, as derived in Leshansky and Kenneth [11]. We discuss the results for each stroke below.

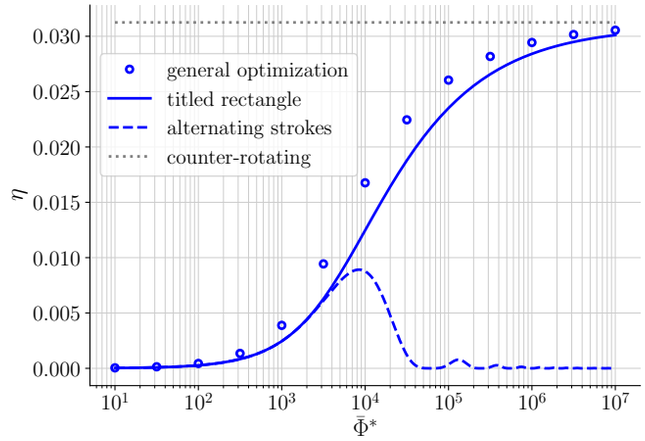

FIG. 3. Optimal efficiency versus the nondimensional average mechanical work $\bar{\Phi}^* = \bar{\Phi}/\left(\mu a^2/T^2\right)$ for the three different gaits, as well as the efficiency of the steady-state counter-rotating cylinder pair[11].

A. Alternating strokes

For the alternating strokes, there exists a global maximum in efficiency at a finite value of nondimensional average mechanical power $\bar{\Phi}^*$. Furthermore, the plot shows a series of local maxima and minima beyond the global optimum, which is a result of the nature of the alternating strokes. Each part of this stroke leads to a circular arc trajectory of the center of mass of the cylinder pair, and so the complete path of the center of mass during a swimming cycle consists of four connected arcs. At the optimum (Fig. 4, solid black line), each circular arc sweeps about 2.28 rads, close to three quarters of a semicircle. The sinusoidal nature of the alternating strokes leads to several local peaks that coincide with similar motions as the global optimum, but with multiple additional complete rotations within each part of the stroke (Fig. 4, gray line). Troughs appear in between, for instance in the case where each circular arc is exactly a circle – in this case, no net motion is achieved and the efficiency is identically zero (Fig. 4, dashed line).

B. Tilted-rectangle strokes

For the general TR strokes, the optimal efficiency η_{TR} increases as a function of the nondimensional average mechani-

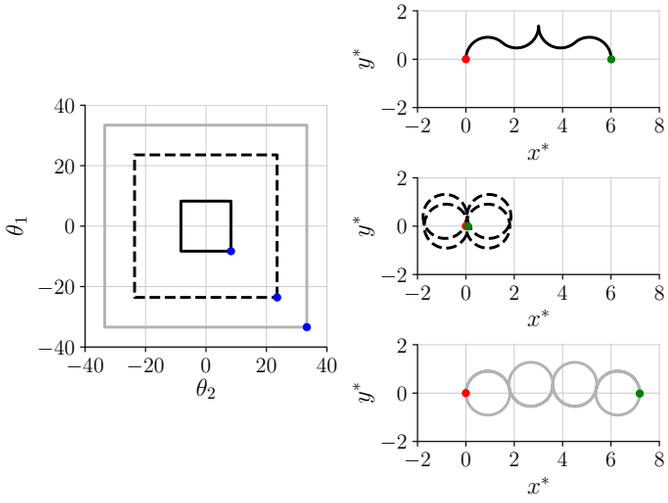

FIG. 4. The multiple local extrema of the alternating strokes. The black solid line is for the global maximum, the dashed black line for the first local minimum (trough), the solid gray line for the first local maximum (peak). The blue dots in the phase space (left figure) denote the start and end points of the phase diagrams. The red and green dots in the figures in the right column denote the start and end points of the physical trajectories. All lengths are scaled with cylinder radius a.

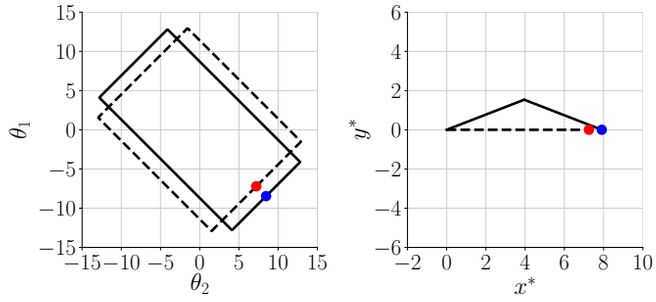

FIG. 5. Comparison between the optimal case with unrestricted α (solid line) and the optimal case with $\alpha = \pi$ (dashed line) for the TR strokes for the same nondimensional average mechanical power $\bar{\Phi}^* = \bar{\Phi}/\left(\mu a^2/T^2\right) = 10^4$. The red and blue dots in the phase space (left column) show the start and end points of the phase diagrams. The red and blue dots in the physical space (right column) show the end points of physical trajectories, for the case with $\alpha = \pi$ and the case with unrestricted α, respectively. All lengths are scaled with cylinder radius a.

cal power $\bar{\Phi}^*$, asymptoting to the value of the counter-rotating efficiency from below as shown in Fig. 3. The optimal strokes exploit the fact that the counter-rotating gait $\dot{\theta}_1 = -\dot{\theta}_2$ is the most efficient way to move, and so the phase space diagrams correspond to rectangles that keep elongating with increasing $\bar{\Phi}^*$.

Interestingly, the value of the turning angle α for the optimal efficiencies is always slightly less than π (shown in Fig. 12 in Appendix C), i.e. the cylinder pair does not perform a complete flip when traversing the short axes of the rectangle in phase space. Figure 5 shows a comparison between an optimal case with unrestricted α (solid lines), and an optimal case where $\alpha = \pi$ (dashed lines). The trajectory of the unrestricted case is skewed and therefore a longer distance needs to be traversed for the same net displacement compared to the restricted case. However, the slight reduction in energy used during the turning maneuver can now be used during the counter-rotating phase, leading to a net displacement of the unrestricted pair that is slightly higher than that of the restricted pair. Also as $\bar{\Phi}^*$ increases, the optimal turning angle α approaches π from below (shown in Fig. 12 in Appendix C), which means the optimal physical trajectory gets closer and closer to a straight line with larger energy budgets.

C. Smooth parametric strokes

Fig. 3 shows that the optimal parametric strokes outperform the tilted-rectangle strokes for all values of $\bar{\Phi}^*$, and also asymptote to the efficiency value of a steadily counter-rotating cylinder pair. To understand why the TR strokes are suboptimal, we compare the physical trajectories and phase diagrams of the TR strokes and the general optimization results at different values of $\bar{\Phi}^*$ in Fig. 6. The cylinder pair with optimized smooth strokes travels farther because the center of mass is always translating and rotating at the same time. To perform a full rotation by π for a given energy budget, our results show that it is more efficient to perform a gait that retains some forward motion, corresponding to a curved phase-space trajectory, than a stationary in-place rotation, corresponding to a straight line in phase-space. At larger values of $\bar{\Phi}^*$, the efficiency is more and more dominated by the counter-rotating part of the gait, and so the distinction between the optimal smooth and optimal tilted rectangle gaits disappears as both asymptote towards the efficiency of the counter-rotating cylinder pair.

V. COUNTER-ROTATION OF 3D CYLINDER WITH SPHERICAL END CAPS

The 2D optimization above shows that the counter-rotating cylinder pair is a simple system with rich complexity in possible gaits. Though the systematic extension of these findings to 3D is beyond the scope of this work, we take a first step to compare the performance of our system to that of other 3D solutions. As mentioned above, in the context of a 3D extension the cylinders can be thought of as the cross-section of a surface-threading torus[11,18], or as a pair of counter-rotating 3D cylinders. We choose to focus on the latter option since it is does not require surface deformations, and is thus arguably the simpler option to consider in an engineering setting.

Our two-dimensional results demonstrate that the efficiency for the periodic gaits is bound from above by the efficiency of a steadily counter-rotating cylinder pair. We therefore focus on finding the corresponding upper bound for efficiency in 3D. Our geometry consists of a cylinder with radius a and length $2(AR-1)a$, where AR is the aspect ratio. The ends

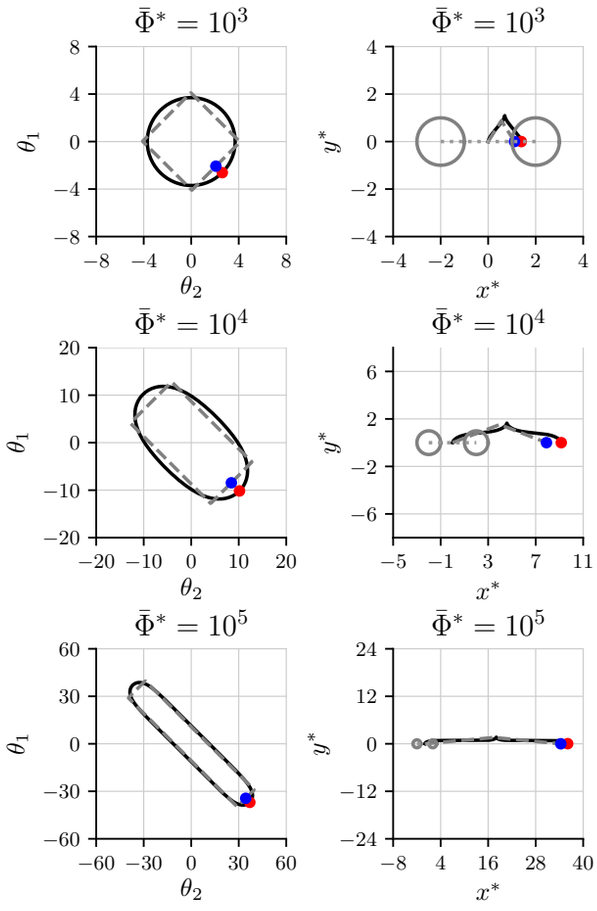

FIG. 6. Comparison of physical trajectories and phase diagrams of the general optimization results using Fourier series (solid lines) and the TR strokes (dashed lines). The red and blue dots in the phase space (left column) show the start and end points of the phase diagrams. The red and blue dots in the physical space (right column) show the end points of physical trajectories. The red dots are for the general optimization results and the blue dots are for the TR strokes. The average mechanical power is nondimensionalized as before i.e. $\bar{\Phi}^* = \bar{\Phi}/\left(\mu a^2/T^2\right)$. All lengths are scaled with cylinder radius a.

of the cylinder are sealed with spherical end caps of radius a (Fig. 7). The cylinders are positioned such that their axes are parallel to each other at a distance $W = 4a$ apart, and they are given equal and opposite angular speeds Ω about their own axes.

To compute the efficiency of these 3D swimmers, we implemented the extension of the method of regularized Stokeslets in three dimensions Cortez, Fauci, and Medovikov [19]. Further, we follow Smith [20] by implementing a constant-force boundary element method where we integrate the 3D stokeslet on each computational element using the Gauss-Legendre quadrature with 12×12 quadrature points. The rest of the numerical methodology is analogous to the 2D case explained above. We consider aspect ratios in the range $2 \leq AR \leq 40$, and for each aspect ratio the cylinders are meshed with around 13000 to 14000 triangular elements each. Since the resolution

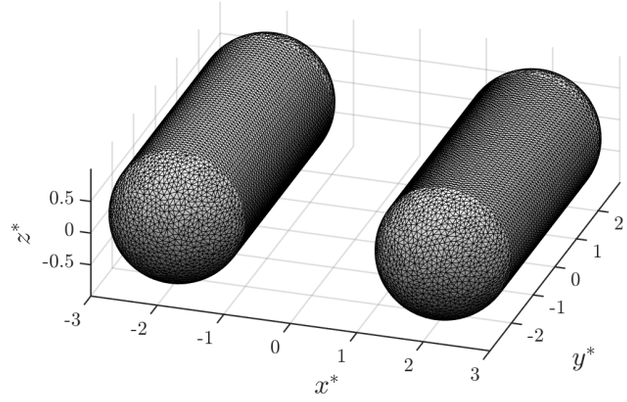

FIG. 7. Plot of the mesh of the 3D cylinder pair with spherical end caps. The aspect ratio $AR = 3$. The axes are scaled such that $x^* = x/a, y^* = y/a, z^* = z/a$. The nondimensional separation between the axes of the cylinders is $W^* = W/a = 4$. For the case shown, each cylinder has 13528 triangular faces.

is approximately constant across simulations, we fix the regularization parameter to $\varepsilon = 0.01$. An example of the mesh is in shown in Fig. 7 for $AR = 3$.

For this 3D system, we can compute efficiency according to equation (9) since the dragging problem is well-posed. Fig. 8 and Fig. 9 show the efficiency and velocity respectively, as a function of aspect ratio AR for the counter-rotating cylinder pair with $W^* = W/a = 4$. The results suggest that the efficiency for a 3D cylinder pair peaks at $\eta' \approx 0.0085$ at a finite aspect ratio of $AR_{\text{opt}} \approx 10$, and the velocity approaches that for a 2D counter-rotating cylinder pair as the aspect ratio increases. We verified that using a '2D' measure of efficiency, analogous to equation (10), the 3D results also approaches the 2D value with increasing AR (details in Appendix E).

Knowing that these efficiency values provide an upper bound for arbitrary gaits of the 3D cylinder pair, we can put them into perspective by comparison with other 3D systems. For $10 \leq AR \leq 40$, the range of efficiency is $0.0051 \leq \eta' \leq 0.0085$. These are the values corresponding to $W^* = W/a = 4$, and similar to the 2D case, we expect the efficiency to increase inversely with W^* as we decrease the separation between the cylinders. For comparison, the efficiency of typical biological cells is around 0.01[1], of a fully optimized Purcell's 3 link swimmer around 0.013[15], and of two counter-rotating spheres of radius a with a center-to-center separation $W^* = W/a = 2.05$ is around 0.02[11]. It is understandable that the last efficiency value, corresponding to $AR = 2$ in our notation, is much higher than the efficiency value achieved by our 3D cylinders since the separation between the spheres is much smaller. Investigating the combined effect of AR and W^* on efficiency of this system is left for future work, but based on the 2D and 3D results we expect the counter-rotating 3D cylinder pair to be able to achieve efficiencies beyond the above reference values.

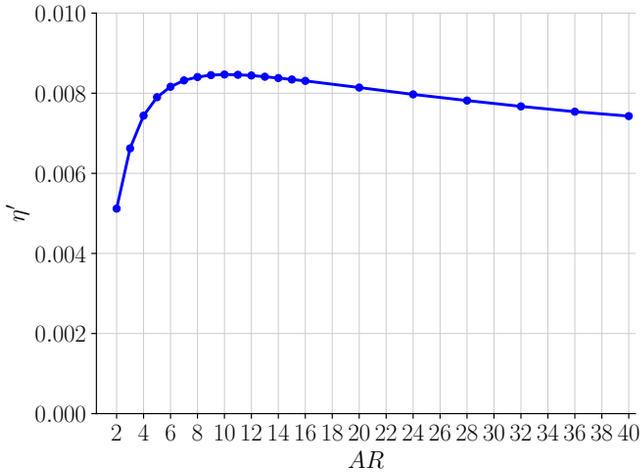

FIG. 8. Efficiency η' of a counter-rotating 3D cylinder pair with spherical end caps for a range of aspect ratio AR.

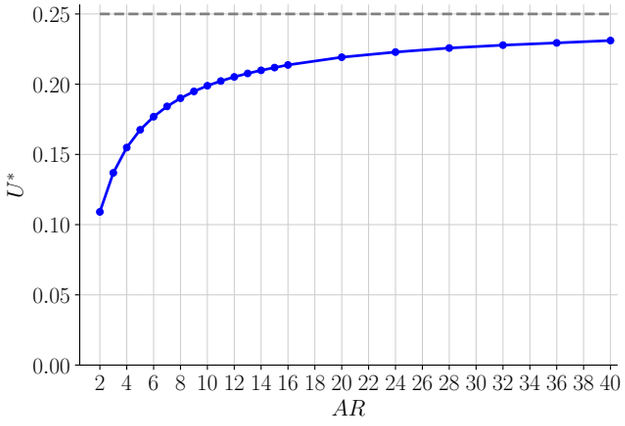

FIG. 9. The nondimensional velocity $U^* = U/(\Omega a)$ vs the aspect ratio AR. The dashed lines denote the corresponding velocities for a 3D cylinder pair with spherical end caps counter-rotating with unit speed, i.e. $U^*_{2D} = 1/W^* = 0.25$.

VI. CONCLUSION

In this work we studied the behavior of a cylinder-pair model swimming using three types of periodic gaits in a low Reynolds number environment. The alternating strokes, inspired by Purcell's three link swimmer, result in trajectories consisting of circular arc segments, and achieve a global maximum in efficiency at a finite value of the average mechanical power $\bar{\Phi}^*$. The TR strokes, which alternate co-rotation and counter-rotation phases, result in trajectories consisting of two straight line segments, and outperform the alternating strokes. For increasing values of $\bar{\Phi}^*$, the efficiency of the TR strokes asymptote towards that of a steadily counter-rotating cylinder pair. Finally, optimal smooth gaits have been found numerically for a range of $\bar{\Phi}^*$ values, leading to trajectories that alternate counter-rotating phases with smooth changes in orientation. The efficiencies of the smooth gaits outperform those of TR strokes, and also asymptote to the steady counter-rotating efficiency limit with increasing $\bar{\Phi}^*$. Lastly, to investigate a simple extension of this geometry to 3D, we computed the efficiency of a counter-rotating pair of 3D cylinders with spherical end caps. The results show that the efficiency is competitive compared with other model systems and the velocity asymptotes to the value for a 2D cylinder pair as the aspect ratio increases.

Beyond this work, we believe that the simplicity of the 3D cylinder pair, both in its geometry and actuation, makes it an attractive model system for both theoretical studies and practical applications of low Reynolds number applications. Different extensions can be easily examined, such as investigating unsteady gaits in the inertial regime[13], employing three or more cylinders and analyzing their optimal configuration in 3D, and broadening to applications beyond locomotion, by using the flow induced by the counter-rotating cylinders for sensing and mixing.

ACKNOWLEDGMENTS

WMvR thanks the MIT Department of Mechanical Engineering for partial financial support of this work.

DATA AVAILABILITY STATEMENT

The data that support the findings of this study are available from the corresponding author upon reasonable request.

Appendix A: The coefficients A_1, A_2, B_1, B_2

For a cylinder pair that is counter-rotating with rotational velocity Ω, we have exact solutions for the translational speed $v_{\text{com}} = \frac{a^2\Omega}{W}$ and power $\bar{\Phi} = 8\pi\mu a^2\Omega^2$[11,12]. In the notation of this work, we can then extract the following equalities:

$$A_1^* = \frac{1}{2W^*}, \tag{A1}$$

$$2B_1^* - B_2^* = 8\pi, \tag{A2}$$

where we set the nondimensional angular speed $\Omega^* = 1$.

To compare, we compute the coefficients A_1^*, A_2^*, B_1^*, B_2^* using the method of regularized Stokeslets described in Section I in MATLAB with $N = 300$ equally spaced discretization points on each cylinder and regularization parameter $\varepsilon = \pi/N$. The results are shown in Fig. 10 and Fig. 11. In the subplot of A_1^* vs W^* in Fig. 10, the numerical values of A_1^* agrees well with the exact values $A_1^* = \frac{1}{2W^*}$. This indicates that the numerical method computes the velocity of the center of mass accurately. In Fig. 11 we notice that the numerical value of $2B_1 - B_2$ diverges away from the exact value 8π for small W^*. The regions $W^* < 4$ in the subplots of B_1^* and B_2^* are shaded

to indicate the region where the results are increasingly incorrect. This divergence is still seen for higher spatial resolutions and other choices of regularization length, implying an $\mathcal{O}(1)$ error for scenarios when the counter-rotating cylinders get increasingly close to each other. We attribute this to our use of a point-wise regularization of the singular Stokeslets, as opposed to the more accurate boundary-integral formulation described in Cortez [14]. For our case of interest, however, we have $W^* = 4$ and our simple numerical method gives an error of 1.2% in $2B_1^* - B_2^*$, which we deem acceptable for our analysis.

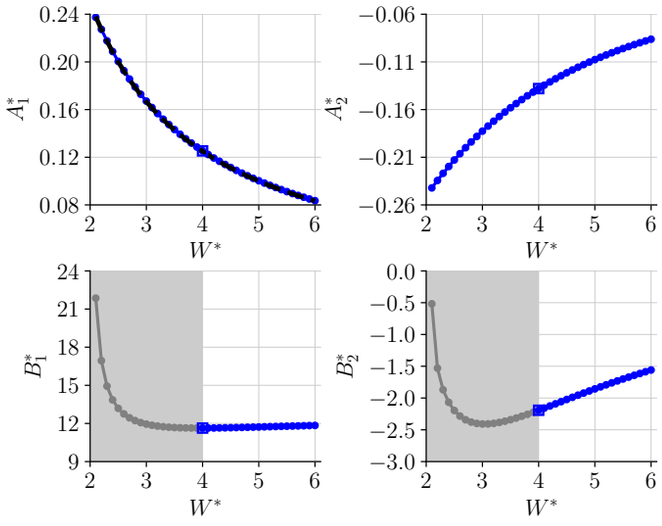

FIG. 10. Numerical values of the nondimensional constants A_1^*, A_2^*, B_1^*, B_2^* for a range of non-dimensional gap sizes W^* are shown in blue lines with markers. For nondimensionalization we have chosen the cylinder radius a as our length scale and $\mu a^2/T^2$ as the scale of power (so $A_1^* = A_1/a$, $A_2^* = A_2$, $B_1^* = B_1/(\mu a^2)$,$B_2^* = B_2/(\mu a^2)$). The spatial resolution used is $N = 600$ and $\varepsilon = \pi/N$. The analytic result of A_1^* is shown in the top left figure in a black dashed line. The large open squares denote the geometry considered here, where $W^* = W/a = 4$. The regions $W^* < 4$ are shaded in the two subplots for B_1^* and B_2^* to indicate that the numerical results are incorrect.

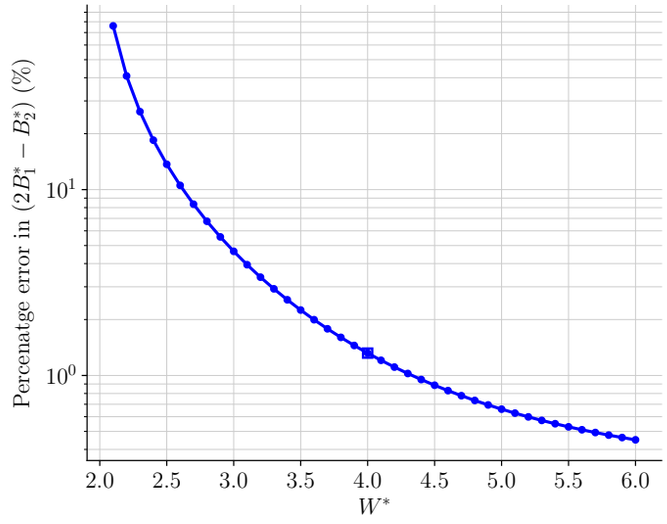

FIG. 11. The percentage error in $2B_1^* - B_2^* = (2B_1 - B_2)/(\mu a^2)$ versus $W^* = W/a$. The analytic value of $2B_1^* - B_2^*$ is known to be a constant equal to 8π. For $W^* = 4$, the percentage error in the numerically computed $2B_1^* - B_2^*$ is 1.2068% (denoted by the blue square).

Appendix B: Alternating stroke

For the alternating stroke, the rotational velocities of each cylinder are defined in equation (16). From this we can compute

$$\dot{\theta}_{\text{com}} = A_2(\dot{\theta}_1 + \dot{\theta}_2) = A_2\dot{\theta}_{\text{alt}} \begin{cases} +1 & \text{if } 0 < t \le \frac{1}{4} \\ -1 & \text{if } \frac{1}{4} < t \le \frac{3}{4} \\ +1 & \text{if } \frac{3}{4} < t \le 1 \end{cases}. \tag{B1}$$

$$v_{\text{com}} = A_1(\dot{\theta}_1 - \dot{\theta}_2) = A_1\dot{\theta}_{\text{alt}} \begin{cases} +1 & \text{if } 0 < t \le \frac{1}{2} \\ -1 & \text{if } \frac{1}{2} < t \le 1 \end{cases}. \tag{B2}$$

Integrating to find the orientation of the cylinder pair, we find

$$\theta_{\text{com}}(t) = \int_0^t \dot{\theta}_{\text{com}}(\tilde{t})\, \mathrm{d}\tilde{t} \tag{B3}$$

$$= A_2\dot{\theta}_{\text{alt}} \begin{cases} t & \text{if } 0 < t \le \frac{1}{4} \\ \frac{1}{2} - t & \text{if } \frac{1}{4} < t \le \frac{3}{4} \\ t - 1 & \text{if } \frac{3}{4} < t \le 1 \end{cases}. \tag{B4}$$

Using the instantaneous orientation $\theta_{\text{com}}(t)$, we can compute the instantaneous lab-frame velocity as

$$\mathbf{u}_{\text{com}}(t) = [-\sin(\theta_{\text{com}}(t))\hat{\mathbf{e}}_x + \cos(\theta_{\text{com}}(t))\hat{\mathbf{e}}_y]A_1(\dot{\theta}_1(t) - \dot{\theta}_2(t)). \tag{B5}$$

The displacement of the center of mass during a cycle is

$$\mathbf{x}_{\text{com}}(t=1) = \int_0^1 \mathbf{u}_{\text{com}}(\tilde{t})d\tilde{t} = -\frac{4A_1}{A_2}\left[1 - \cos\left(\frac{1}{4}A_2\dot{\theta}_{\text{alt}}\right)\right]\hat{\mathbf{e}}_x, \tag{B6}$$

from which we can directly compute the average velocity $\bar{\mathbf{u}}$. This provides the numerator of the efficiency in equation (10). The denominator was found in the main text as $\bar{\Phi} = B_1\dot{\theta}_{\text{alt}}^2$. The efficiency is then

$$\eta_{\text{alt}}(\bar{\Phi}) = \frac{64\pi\mu}{\bar{\Phi}}\left(\frac{A_1}{A_2}\right)^2\left[1 - \cos\left(\frac{A_2}{4}\sqrt{\frac{\bar{\Phi}}{B_1}}\right)\right]^2. \tag{B7}$$

Appendix C: Tilted-Rectangle stroke

For the tilted-rectangle strokes, the optimal angle α between the length segments defined in Eq. 20 approaches π from below as the non-dimensional average mechanical power $\bar{\Phi}^*$ increases, which is shown in Fig. 12.

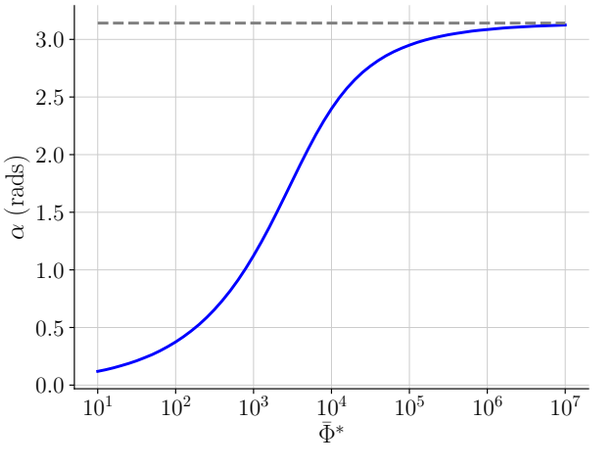

FIG. 12. The angle α in Eq. (20) versus the nondimensional average mechanical power $\bar{\Phi}^* = \bar{\Phi}/\left(\mu a^2/T^2\right)$ for the optimal TR strokes. The gray dashed line denotes the value $\alpha = \pi$.

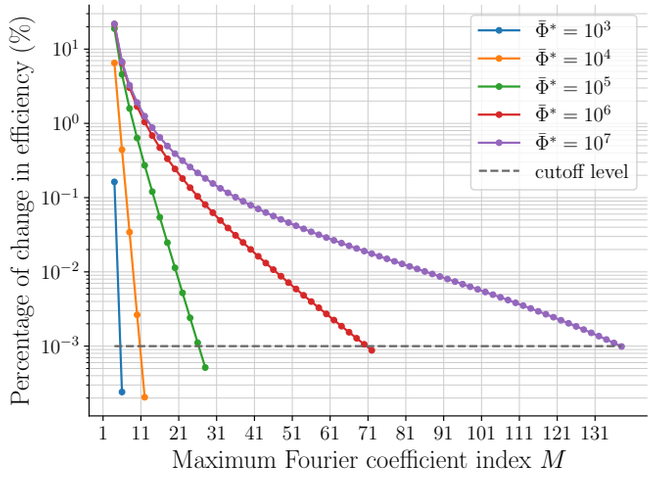

FIG. 13. Percentage change in efficiency versus the maxium Fourier coefficient index M for different nondimensional average mechanical power $\bar{\Phi}^* = \bar{\Phi}/(\mu a^2)$.

Appendix D: Convergence of smooth stroke optimization

To determine how many coefficients are required to obtain a converged result in the optimization of the smooth strokes, we incrementally increase M and perform an optimization for each increment. This allows us to compute the corresponding change in the efficiency, and we consider the result to have converged when this incremental change in the efficiency is less than 0.001%

Figure 13 shows the percentage of change in efficiency as a function of the number of Fourier coefficients used in the efficiency optimization, for various values of $\bar{\Phi}^*$. We chose a threshold of 10^{-3} to determine that the efficiency is unlikely to change significantly if more coefficients will be added. Once that threshold is reached for a given $\bar{\Phi}^*$, we terminate the optimization.

Appendix E: 3D cylinder pair

We can define an efficiency $\eta_{2D} = 4\pi\mu\bar{u}^2(2ARa)/\bar{\phi}$ for the 3D cylinder pair analogous to the 2D case. The values of η_{2D} versus AR are plotted in Fig. 14, where the dashed line denotes the efficiency for a counter-rotating 2D cylinder pair for $W^* = W/a = 4$. It shows that η_{2D} approaches the counter-rotating efficiency value of the 2D cylinder pair, $1/32 = 0.03125$, as the aspect ratio increases.

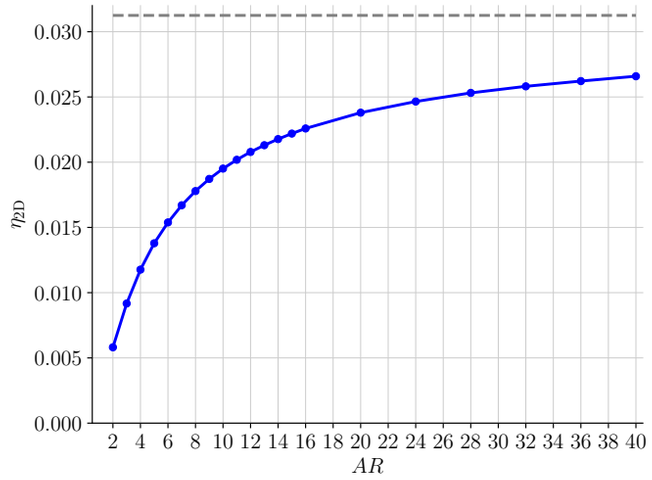

FIG. 14. Efficiency $\eta_{2D} = 4\pi\mu\bar{u}^2(2ARa)/\bar{\phi}$ of a 3D cylinder pair with spherical end caps counter-rotating with unit speed for a range of aspect ratio AR and $W^* = W/a = 4$. The gray dashed line denotes the efficiency value for a 2D counter-rotating cylinder pair with $W^* = W/a = 4$.

[1] E. Lauga and T. R. Powers, "The hydrodynamics of swimming microorganisms," Reports on Progress in Physics **72**, 096601 (2009).
[2] B. J. Nelson, I. K. Kaliakatsos, and J. J. Abbott, "Microrobots for minimally invasive medicine," Annual Review of Biomedical Engineering **12**, 55–85 (2010).
[3] M. Sitti, H. Ceylan, W. Hu, J. Giltinan, M. Turan, S. Yim, and E. Diller, "Biomedical applications of untethered mobile milli/microrobots," Proceedings of the IEEE **103**, 205–224 (2015).
[4] E. M. Purcell, "Life at low Reynolds number," American Journal of Physics **45**, 3–11 (1977).
[5] A. Najafi and R. Golestanian, "Simple swimmer at low Reynolds number: Three linked spheres," Physical Review E **69** (2004), 10.1103/physreve.69.062901.
[6] E. Gutman and Y. Or, "Symmetries and gaits for Purcell's three-link microswimmer model," IEEE Transactions on Robotics **32**, 53–69 (2016).
[7] F. Box, E. Han, C. R. Tipton, and T. Mullin, "On the motion of linked spheres in a Stokes flow," Experiments in Fluids **58** (2017), 10.1007/s00348-017-2321-2.
[8] G. I. Taylor, "Analysis of the swimming of microscopic organisms," Proceedings of the Royal Society of London. Series A. Mathematical and Physical Sciences **209**, 447–461 (1951).
[9] J. Blake, "Self propulsion due to oscillations on the surface of a cylinder at low Reynolds number," Bulletin of the Australian Mathematical Society **5**, 255–264 (1971).

[10]G. I. Taylor, "The action of waving cylindrical tails in propelling microscopic organisms," Proceedings of the Royal Society of London. Series A. Mathematical and Physical Sciences **211**, 225–239 (1952).
[11]A. M. Leshansky and O. Kenneth, "Surface tank treading: Propulsion of purcell's toroidal swimmer," Physics of Fluids **20**, 063104 (2008).
[12]G. B. Jeffery, "The rotation of two circular cylinders in a viscous fluid," Proceedings of the Royal Society of London. Series A, Containing Papers of a Mathematical and Physical Character **101**, 169–174 (1922).
[13]W. M. van Rees, G. Novati, and P. Koumoutsakos, "Self-propulsion of a counter-rotating cylinder pair in a viscous fluid," Physics of Fluids **27**, 063102 (2015).
[14]R. Cortez, "The method of regularized Stokeslets," SIAM Journal on Scientific Computing **23**, 1204–1225 (2001).
[15]D. Tam and A. E. Hosoi, "Optimal stroke patterns for Purcell's three-link swimmer," Physical Review Letters **98** (2007), 10.1103/physrevlett.98.068105.
[16]J. E. Avron, O. Gat, and O. Kenneth, "Optimal swimming at low Reynolds numbers," Physical Review Letters **93** (2004), 10.1103/physrevlett.93.186001.
[17]H. A. Stone and A. D. T. Samuel, "Propulsion of microorganisms by surface distortions," Physical Review Letters **77**, 4102–4104 (1996).
[18]J. Huang and L. Fauci, "Interaction of toroidal swimmers in Stokes flow," Physical Review E **95** (2017), 10.1103/physreve.95.043102.
[19]R. Cortez, L. Fauci, and A. Medovikov, "The method of regularized Stokeslets in three dimensions: analysis, validation, and application to helical swimming," Physics of Fluids **17**, 031504 (2005).
[20]D. J. Smith, "A boundary element regularized Stokeslet method applied to cilia- and flagella-driven flow," Proceedings of the Royal Society A: Mathematical, Physical and Engineering Sciences **465**, 3605–3626 (2009).

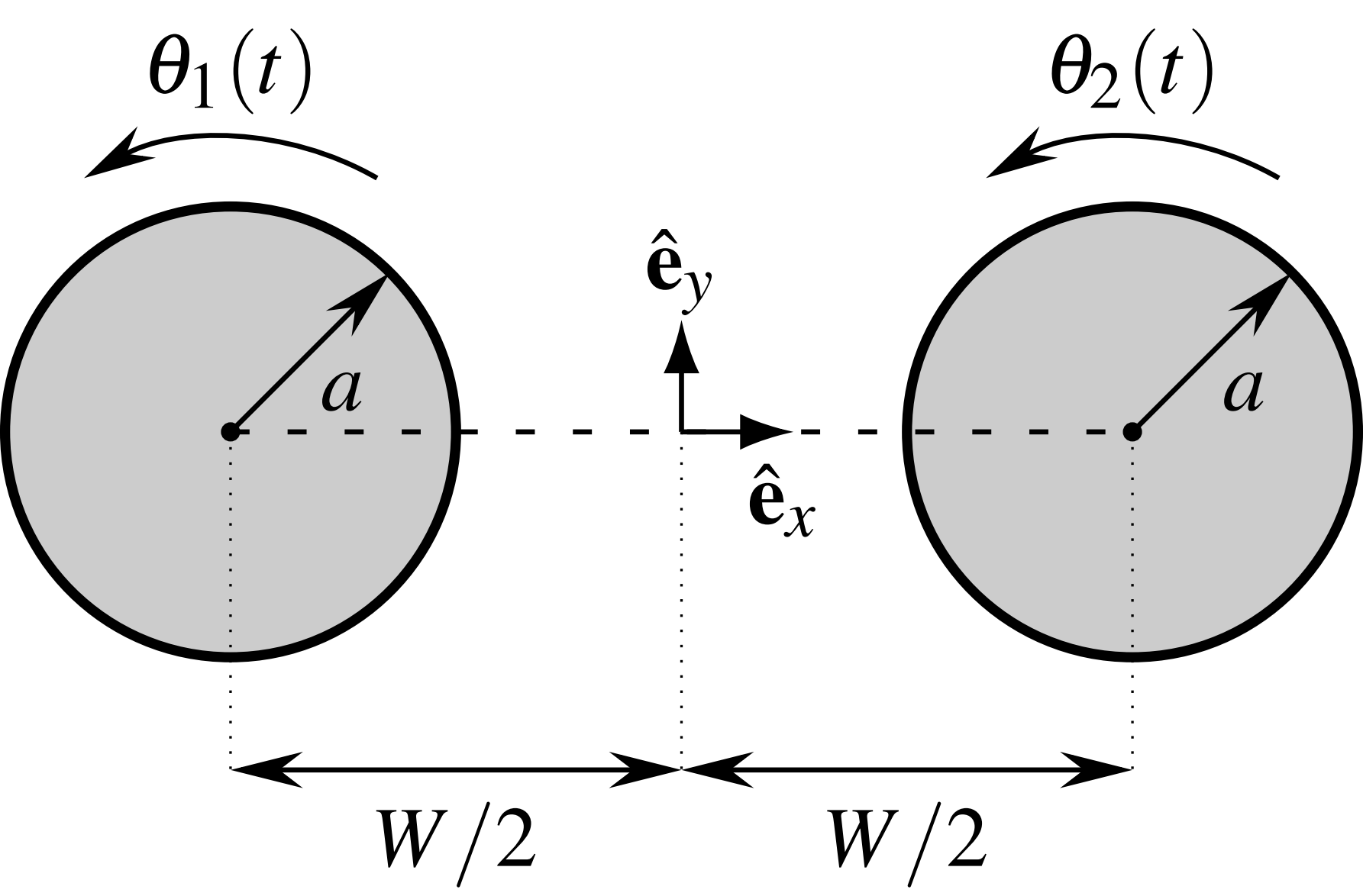
$\theta_1(t)$
$\theta_2(t)$
$\hat{\mathbf{e}}_y$
$\hat{\mathbf{e}}_x$
a
a
$W/2$
$W/2$

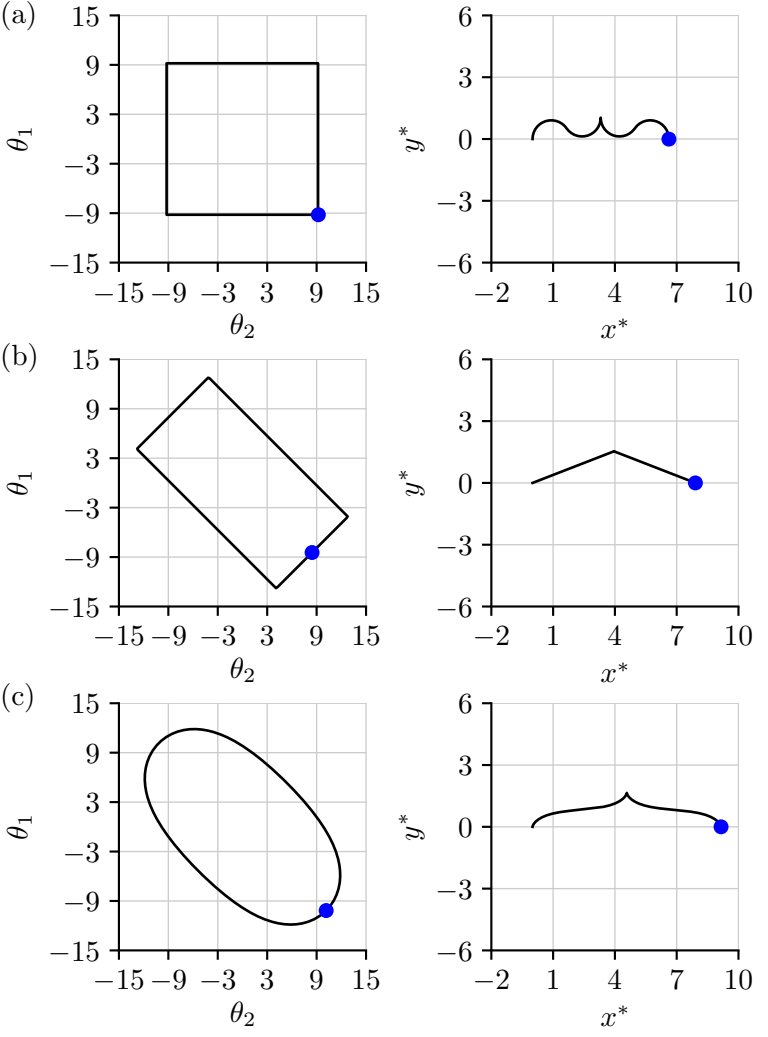
(a)
15
9
3
−3
−9
−15
θ_1
−15 −9 −3 3 9 15
θ_2
6
3
0
−3
−6
y^*
−2 1 4 7 10
x^*
(b)
15
9
3
−3
−9
−15
θ_1
−15 −9 −3 3 9 15
θ_2
6
3
0
−3
−6
y^*
−2 1 4 7 10
x^*
(c)
15
9
3
−3
−9
−15
θ_1
−15 −9 −3 3 9 15
θ_2
6
3
0
−3
−6
y^*
−2 1 4 7 10
x^*

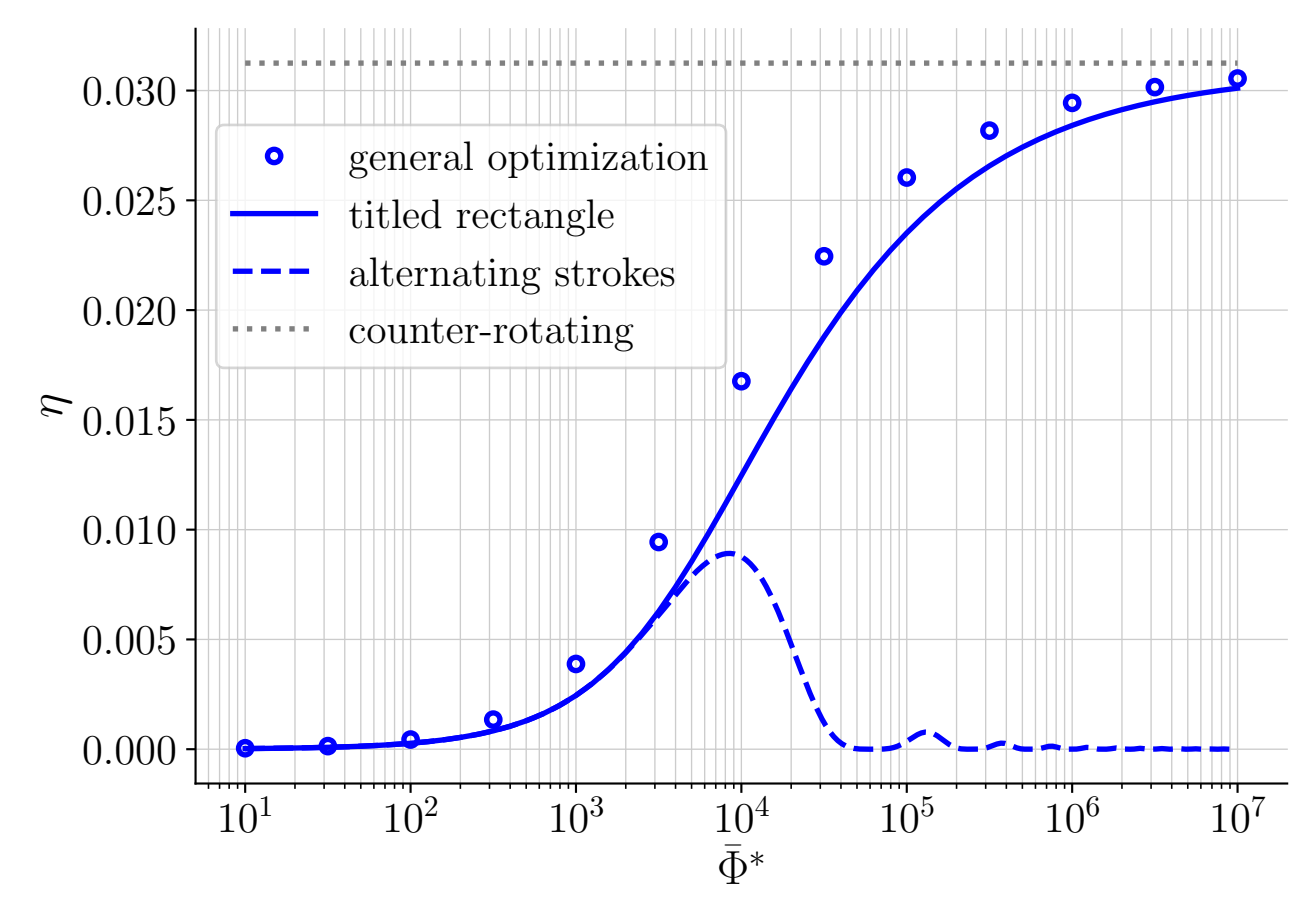
general optimization
titled rectangle
alternating strokes
counter-rotating
η
0.030
0.025
0.020
0.015
0.010
0.005
0.000
10^1
10^2
10^3
10^4
10^5
10^6
10^7
$\bar{\Phi}^*$

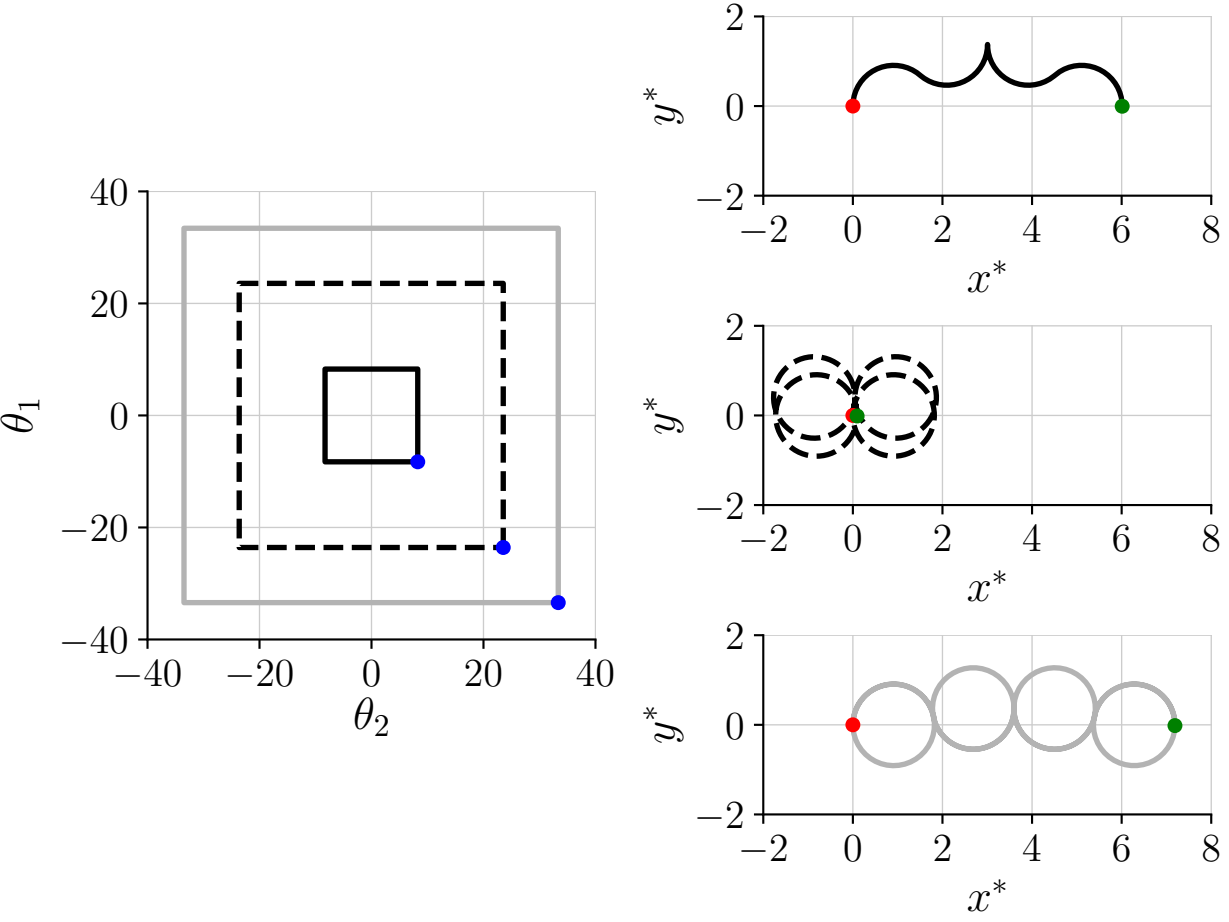
40
20
0
−20
−40
θ_1
−40
−20
0
20
40
θ_2
2
0
−2
y^*
−2
0
2
4
6
8
x^*
2
0
−2
y^*
−2
0
2
4
6
8
x^*
2
0
−2
y^*
−2
0
2
4
6
8
x^*

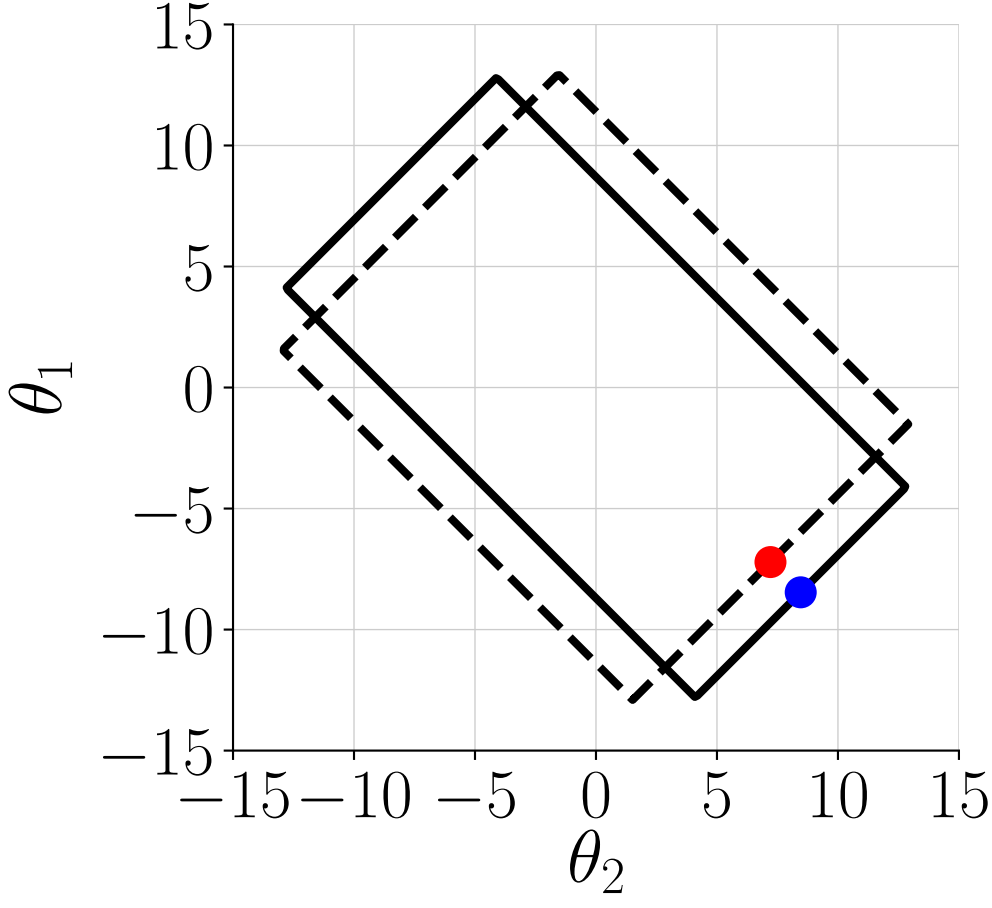
15
10
5
0
−5
−10
−15
θ_1
−15 −10 −5 0 5 10 15
θ_2

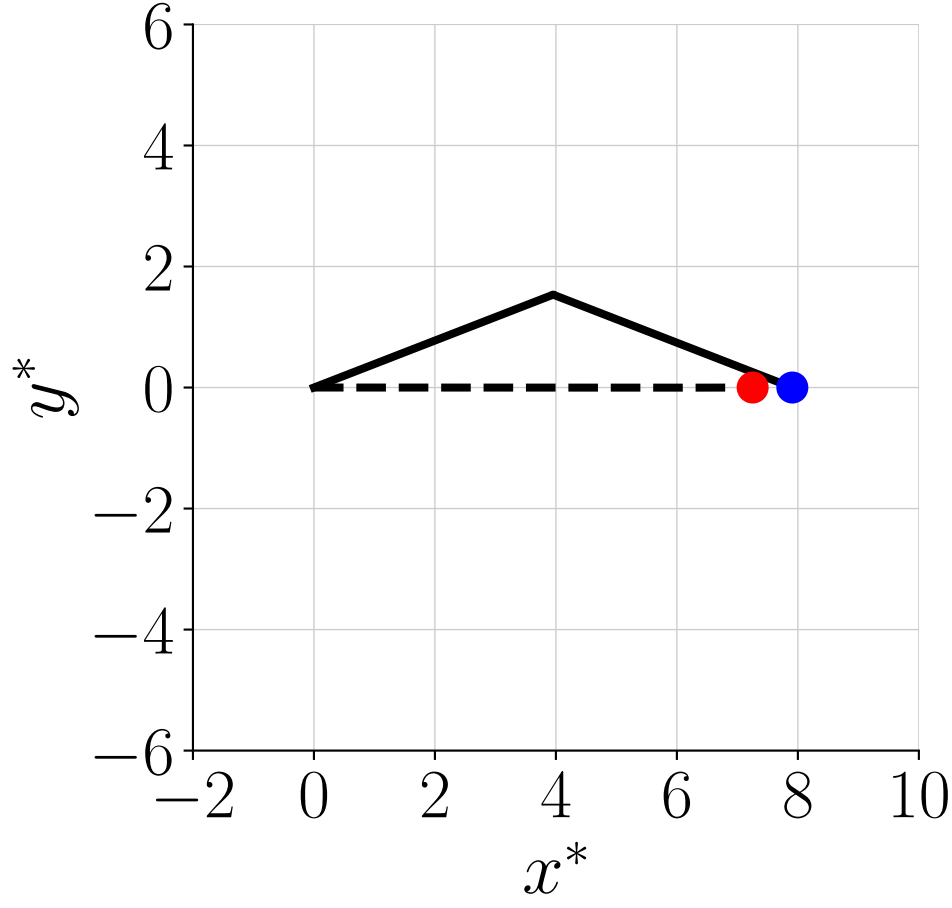
6
4
2
0
−2
−4
−6
y^*
−2 0 2 4 6 8 10
x^*

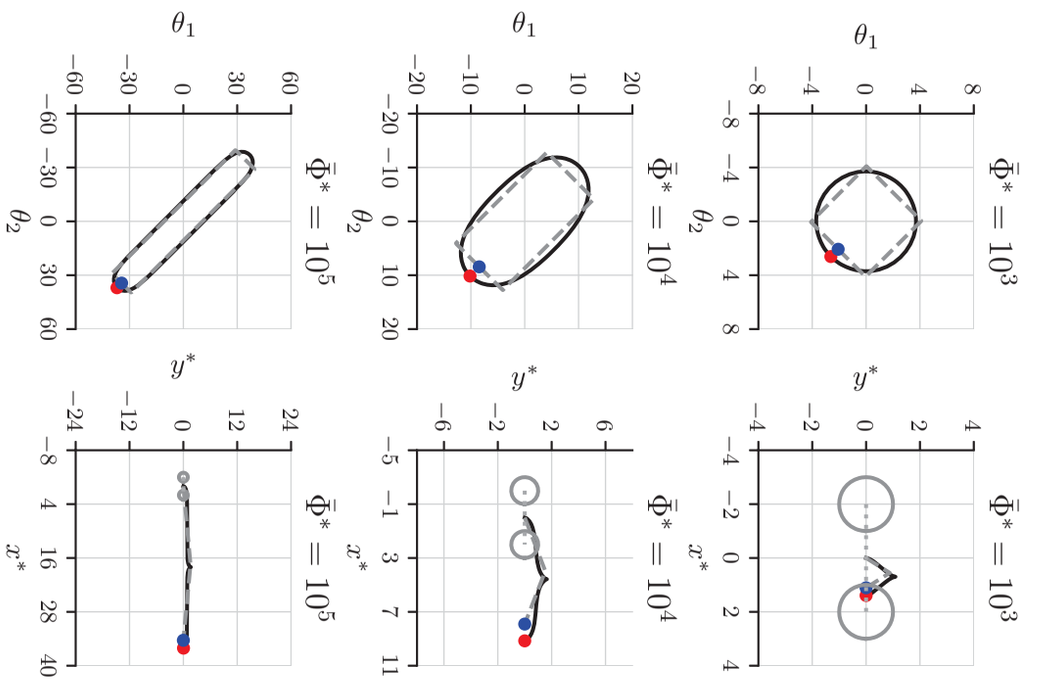

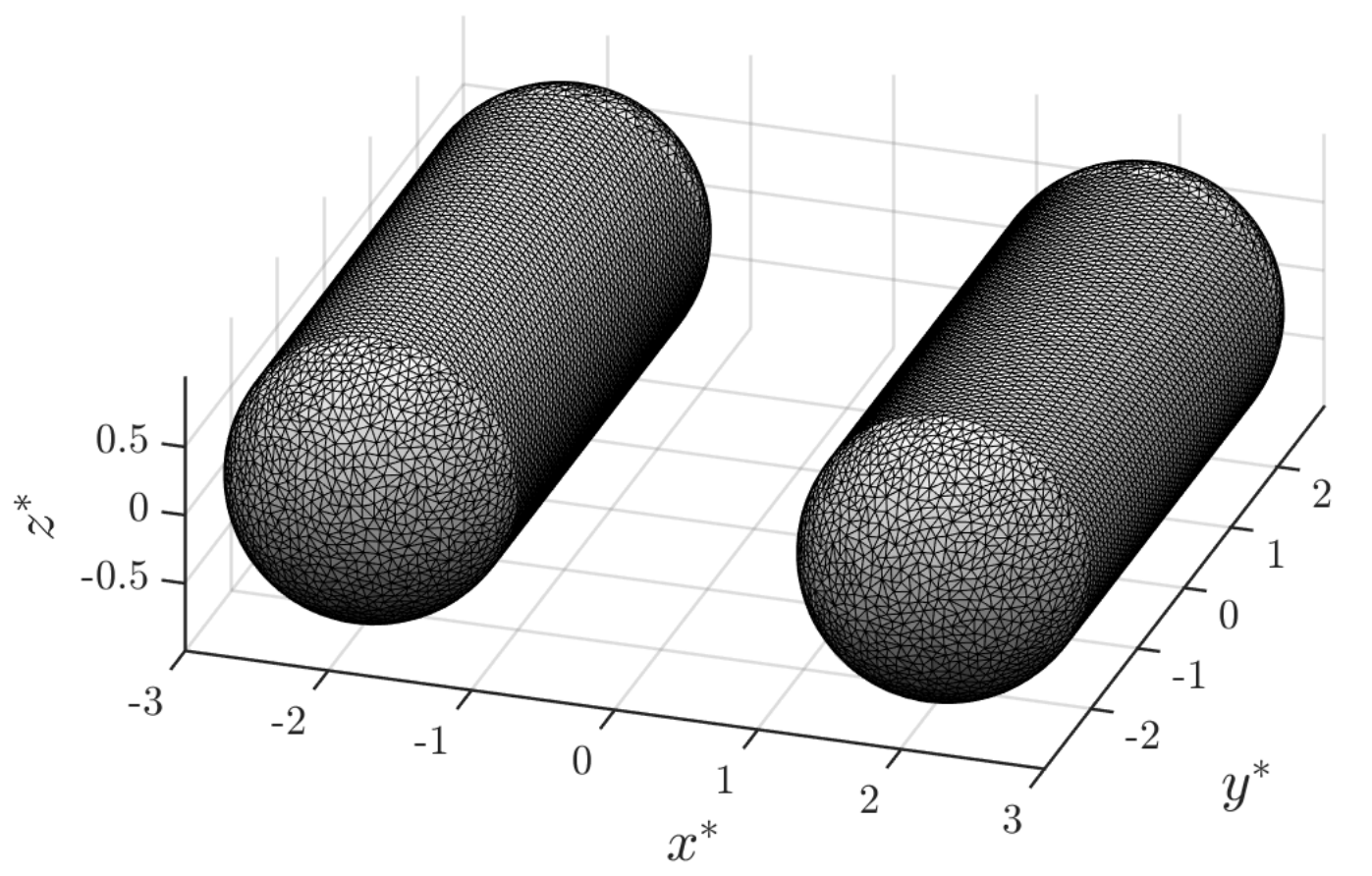
0.5
0
-0.5
z^*
-3
-2
-1
0
1
2
3
x^*
2
1
0
-1
-2
y^*

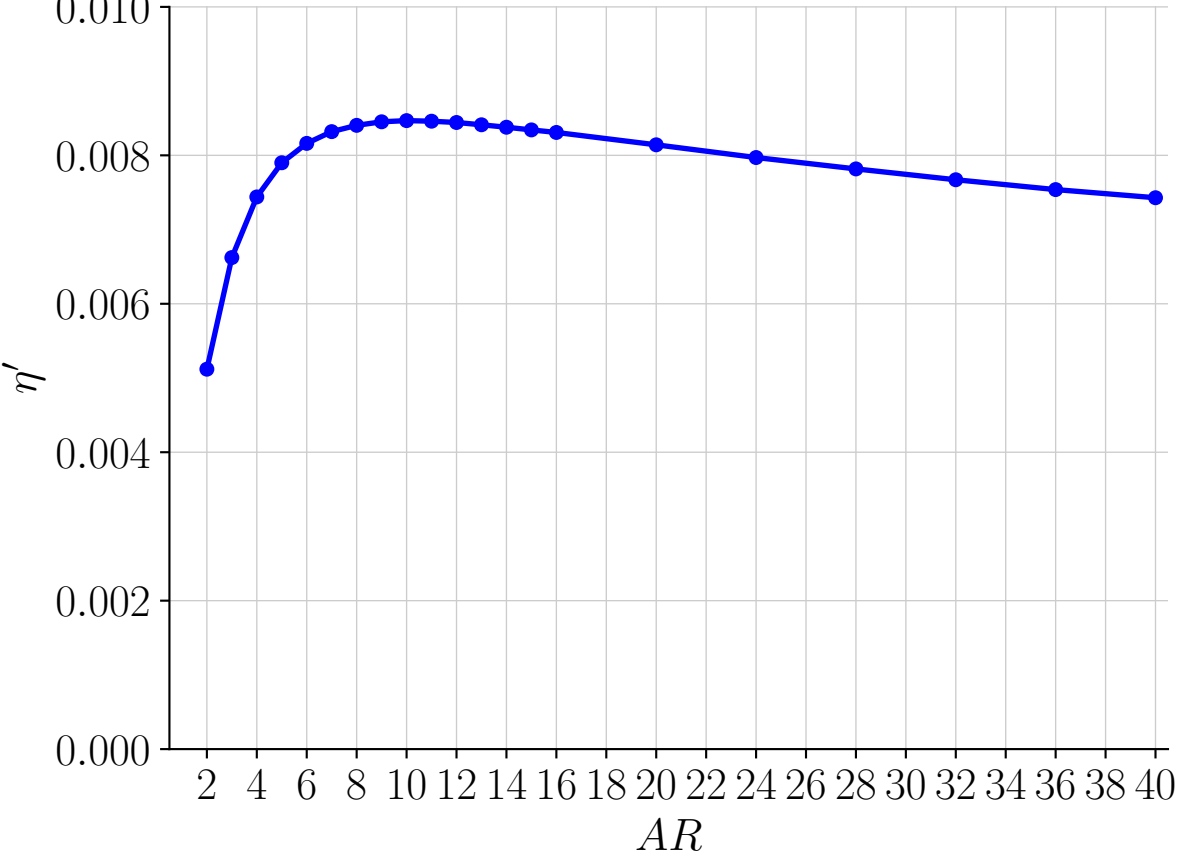
0.010
0.008
0.006
0.004
0.002
0.000
η'
2 4 6 8 10 12 14 16 18 20 22 24 26 28 30 32 34 36 38 40
AR

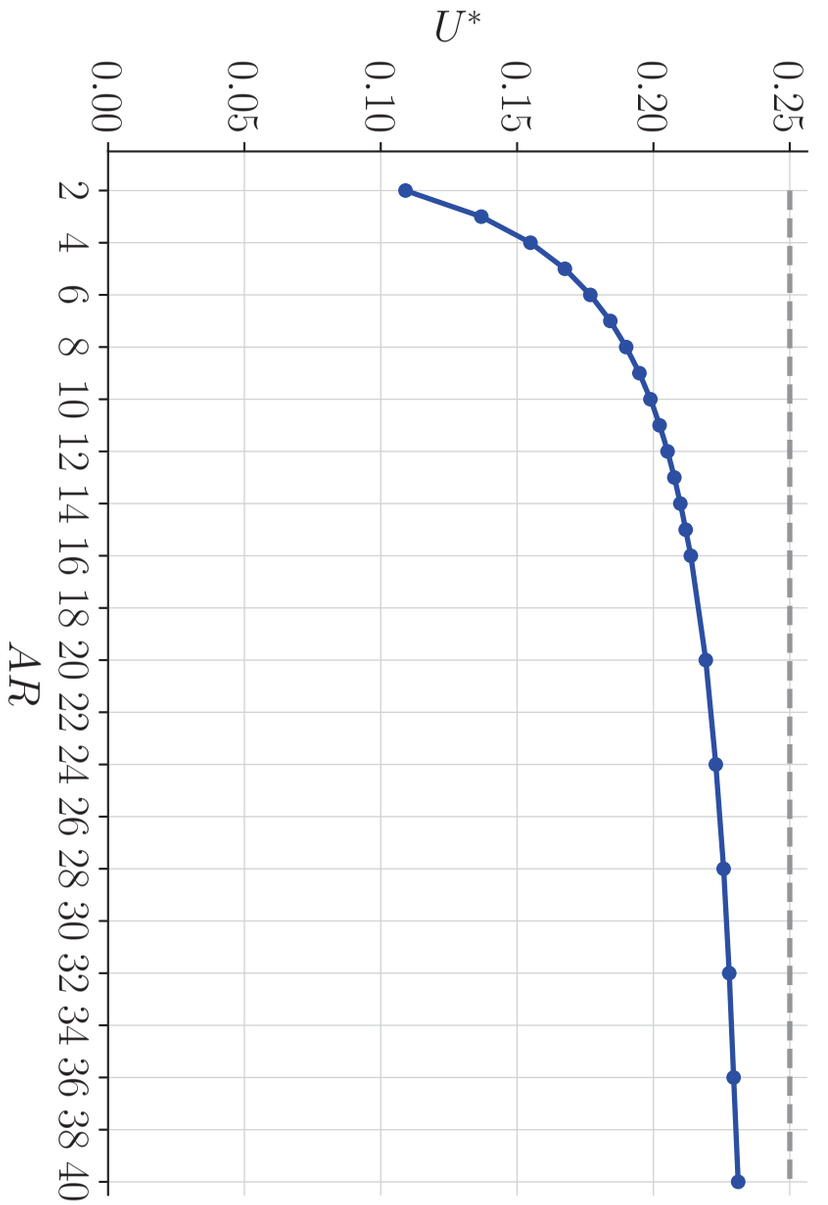

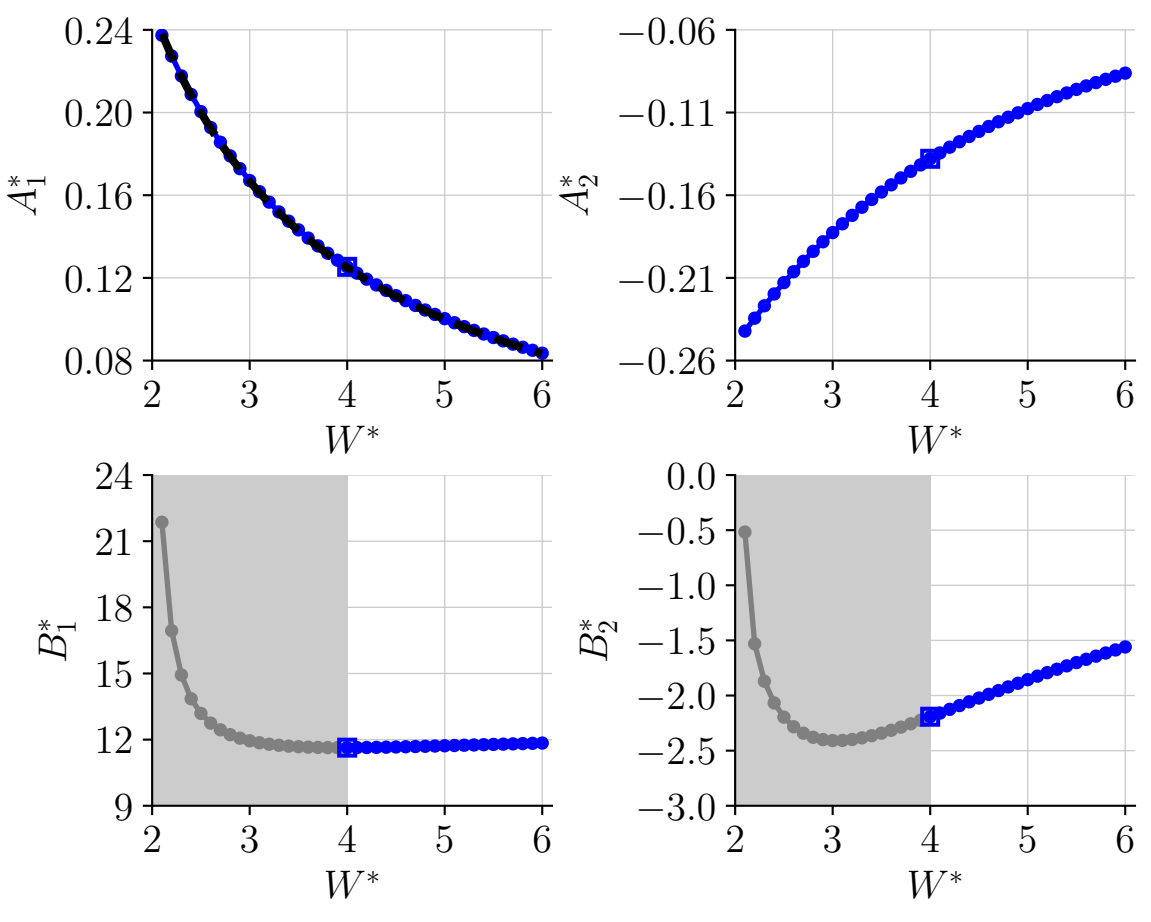
0.24
0.20
0.16
0.12
0.08
A_1^*
2
3
4
5
6
W^*
−0.06
−0.11
−0.16
−0.21
−0.26
A_2^*
W^*
24
21
18
15
12
9
B_1^*
W^*
0.0
−0.5
−1.0
−1.5
−2.0
−2.5
−3.0
B_2^*
W^*

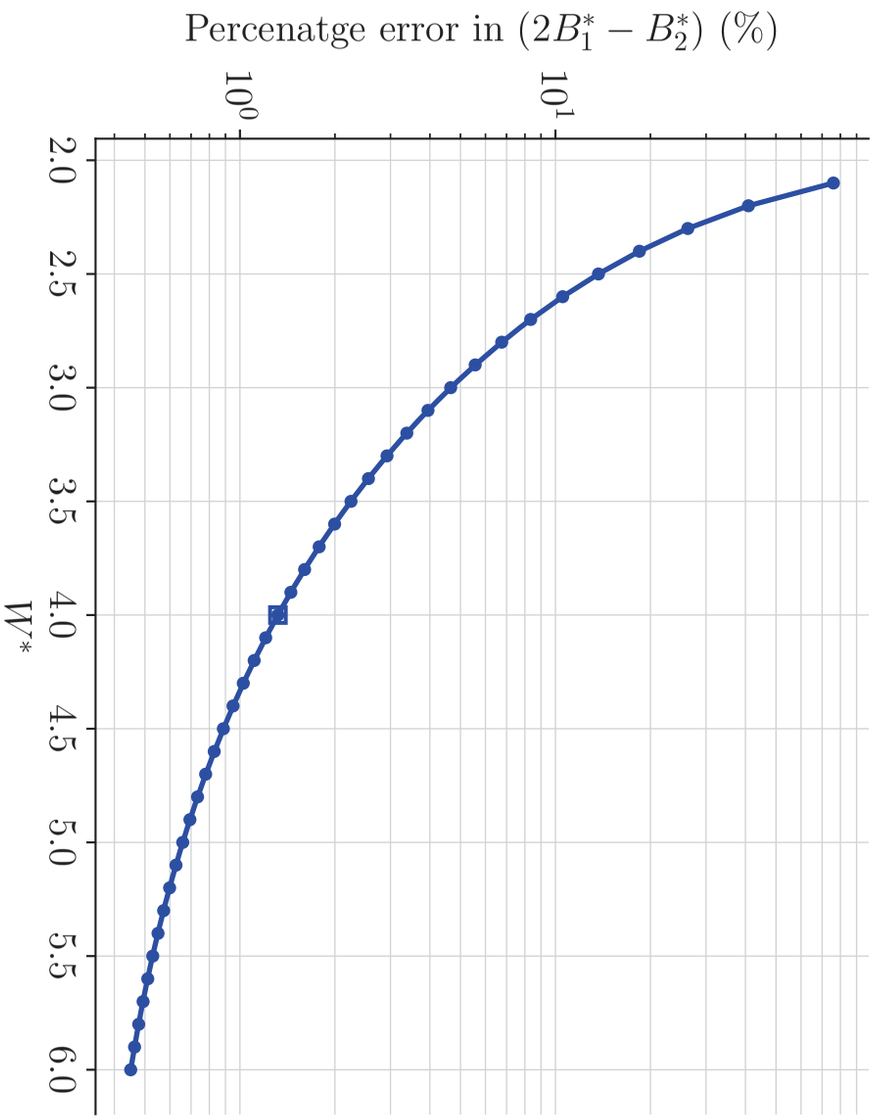

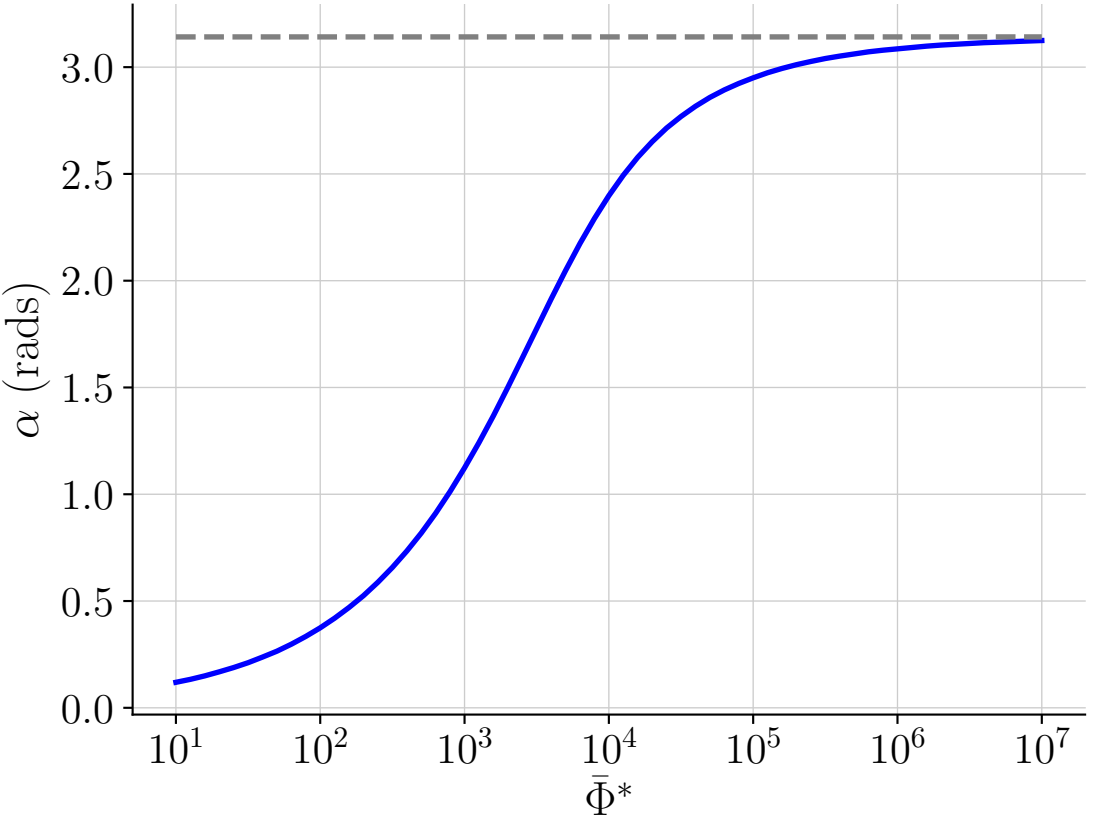
3.0
2.5
2.0
1.5
1.0
0.5
0.0
α (rads)
10^1
10^2
10^3
10^4
10^5
10^6
10^7
$\bar{\Phi}^*$

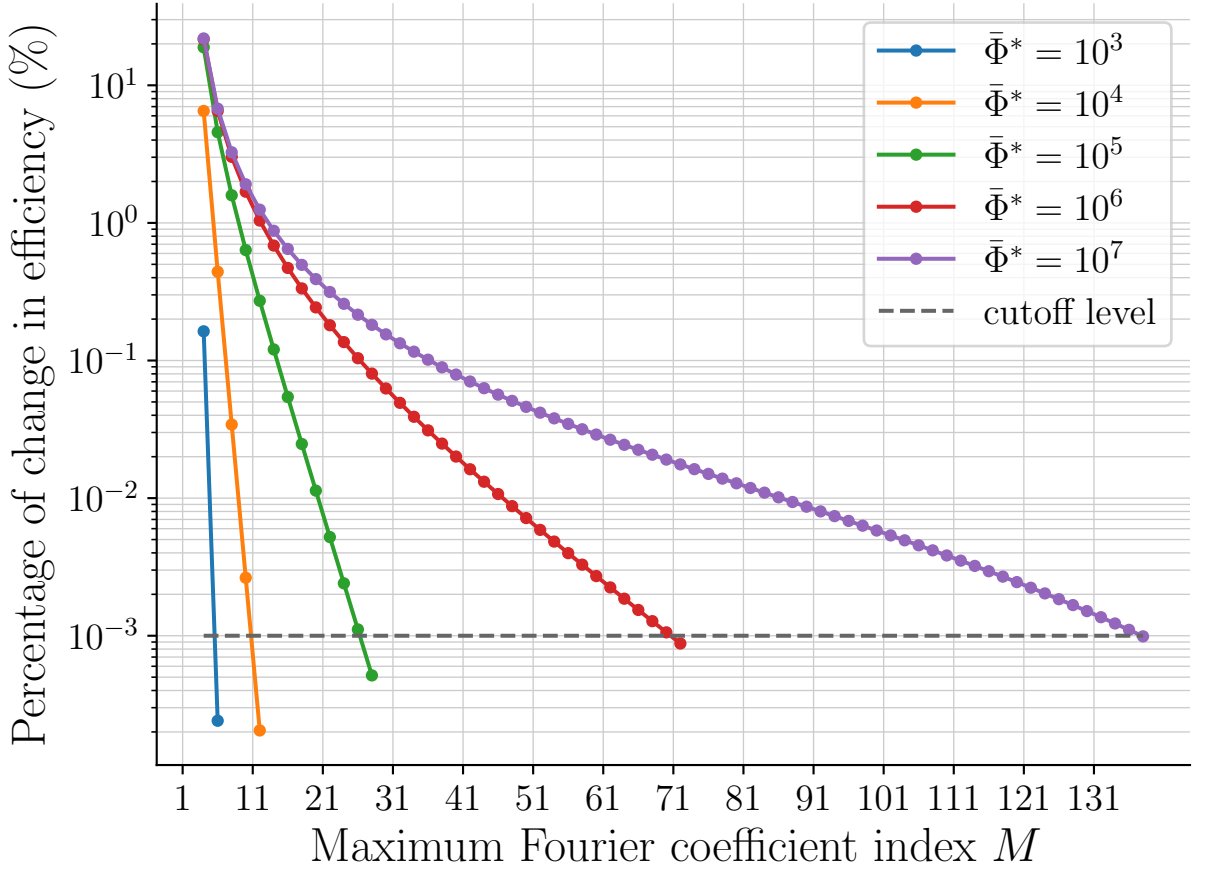
$\bar{\Phi}^* = 10^3$
$\bar{\Phi}^* = 10^4$
$\bar{\Phi}^* = 10^5$
$\bar{\Phi}^* = 10^6$
$\bar{\Phi}^* = 10^7$
cutoff level
Percentage of change in efficiency (%)
10^1
10^0
10^{-1}
10^{-2}
10^{-3}
1 11 21 31 41 51 61 71 81 91 101 111 121 131
Maximum Fourier coefficient index M

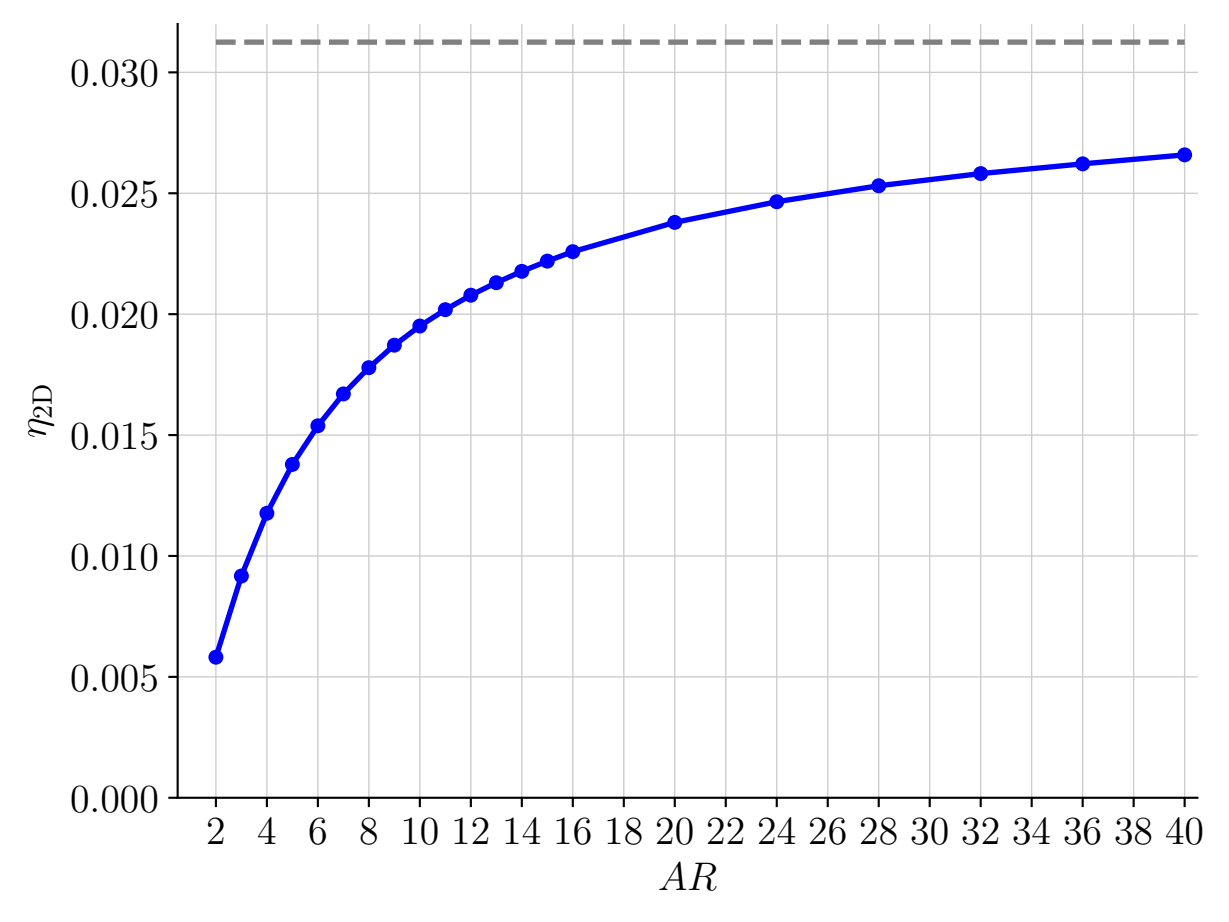
0.030
0.025
0.020
0.015
0.010
0.005
0.000
η_{2D}
2 4 6 8 10 12 14 16 18 20 22 24 26 28 30 32 34 36 38 40
AR